



HAL
open science

**New insight of sedimentological and geochemical
characterization of siliciclastic-carbonate deposits
(Alveolina Limestone Formation, Graus-Tremp basin,
Spain)**

Youri Hamon, Rémi Deschamps, Philippe Joseph, Daniel Garcia, Emmanuelle
Chanvry

► **To cite this version:**

Youri Hamon, Rémi Deschamps, Philippe Joseph, Daniel Garcia, Emmanuelle Chanvry. New insight of sedimentological and geochemical characterization of siliciclastic-carbonate deposits (Alveolina Limestone Formation, Graus-Tremp basin, Spain). Bulletin de la Société Géologique de France, 2016, 187 (3), pp.133-153. 10.2113/gssgfbull.187.3.133 . hal-01311499

HAL Id: hal-01311499

<https://hal.science/hal-01311499>

Submitted on 12 May 2016

HAL is a multi-disciplinary open access archive for the deposit and dissemination of scientific research documents, whether they are published or not. The documents may come from teaching and research institutions in France or abroad, or from public or private research centers.

L'archive ouverte pluridisciplinaire **HAL**, est destinée au dépôt et à la diffusion de documents scientifiques de niveau recherche, publiés ou non, émanant des établissements d'enseignement et de recherche français ou étrangers, des laboratoires publics ou privés.

New insight of sedimentological and geochemical characterization of siliciclastic-carbonate deposits (*Alveolina Limestone Formation, Graus-Tremp Basin, Spain*).

Nouveau regard sur la caractérisation sédimentologique et géochimique d'une série mixte "siliciclastique-carbonate" (la formation des *Calcaires à Alvéolines*, Bassin de Graus-Tremp, Espagne).

*Youri Hamon*¹, *Remy Deschamps*¹, *Philippe Joseph*¹, *Daniel Garcia*², *Emmanuelle Chanvry*^{1,3}

1: IFP Énergies nouvelles, 1 et 4 avenue de Bois-Préau, 92852 Rueil-Malmaison, France

2: Centre SPIN, Ecole Nationale Supérieure des Mines de Saint Etienne, and UMR CNRS 5600, 158 cours Fauriel, 42023 Saint-Etienne, France

3: TOTAL SA, CSTJF, avenue Larribau, 64018 Pau, France

Corresponding author: youri.hamon@ifpen.fr

15

Keywords / Mots Clés :

Mixed facies; isotopes; elemental geochemistry; exposure; sequence stratigraphy; Ilerdian.

Faciès mixtes ; isotopes ; géochimie élémentaire ; émergence ; stratigraphie séquentielle ; Ilerdien.

Abstract:

This article is a first attempt of combining sedimentological analysis and geochemical systematics of the *Alveolina Limestone* Formation as a tool to identify the major stratigraphic surfaces, and to improve the sequence stratigraphy interpretation. This formation is Early Eocene in age and crops out in several well-exposed cliffs in the Serraduy - Roda de Isabena area (Graus-Tremp Basin, NE Spain). Within this succession, nineteen carbonate and siliciclastic facies have been identified and grouped in environmental facies associations (based on their vertical stacking and lateral relationships): 1) coastal plain; 2) clastic deltaic complex; 3) shallow carbonate inner-ramp; 4) mid-ramp; 5) outer-ramp; 6) reefal facies. The depositional architectures studied in the Serraduy area can be directly assessed on the field, and a 3D reconstruction is proposed. This enables us to build a synthetic depositional model and to identify five small-scale T/R cycles, bounded by different kinds of sedimentary discontinuities: angular unconformity, firmground, erosional surface... In parallel, geochemical analyses (C and O isotopes, major, minor and trace elements) were carried out to help at hierarchizing the cycles and the boundaries previously identified. Four of them may be considered as major stratigraphic surfaces, corresponding either to regional-scale angular unconformity, or to exposure surfaces. The latter are characterized by a selective dissolution, a slight but sharp decrease in $\delta^{13}\text{C}_{\text{V-PDB}}$ and in Mg, Fe and Sr contents below the surface. The absence of typical sedimentary criteria of exposure (with the exception of these geochemical signatures) may be explained by short-term exposure, an arid to semi-arid climate, and a dominant low-magnesian calcite original mineralogy, precluding the development and the preservation of widespread vadose diagenetic products. A new sequence stratigraphy model for the *Alveolina Limestone Fm* is finally proposed and discussed.

Résumé:

Cet article propose une étude intégrée, sédimentologique et géochimique, utilisée en tant qu'outil pour identifier les surfaces à valeur stratigraphique majeure et pour améliorer les interprétations de stratigraphie séquentielle. L'étude est réalisée sur la formation des « Calcaires à *Alvéolines* », d'âge Eocène Inférieur qui affleure de manière spectaculaire dans la région de Serraduy - Roda de Isabena (Bassin de Graus-Tremp, NE de l'Espagne). Au sein de cette succession, dix-neuf faciès (tant siliciclastiques que carbonatés) ont été identifiés et regroupés en associations de faciès caractéristiques d'environnements de dépôt, en se basant sur leur empilement vertical et leurs relations latérales : 1) plaine côtière ; 2) complexe siliciclastique deltaïque ; 3) rampe carbonatée interne peu profonde ; 4) rampe médiane ; 5) rampe externe ; 6) faciès récifaux. Les architectures de dépôt peuvent être directement évaluées sur le terrain et une reconstruction 3D est proposée. Ces points ont permis d'établir un modèle de dépôt synthétique et d'identifier cinq cycles élémentaires transgressifs/régressifs, délimités par différents types de discontinuités sédimentaires : discordance, surface durcie, surface d'érosion... En parallèle, des analyses géochimiques (isotopes du carbone et de l'oxygène, géochimie des majeurs, mineurs et traces) ont été menées afin d'aider à la hiérarchisation des cycles élémentaires et de leurs limites. Quatre d'entre elles peuvent être considérées comme des surfaces stratigraphiques majeures, correspondant soit à des discordances angulaires d'échelle régionale, soit à des surfaces d'émersion. Ces dernières se caractérisent par une dissolution sélective, une chute légère en $\delta^{13}\text{C}_{\text{V-PDB}}$, ainsi qu'en Mg, Fe et Sr, sous la surface. L'absence de critère sédimentaire d'émersion (à l'exception de ces signaux géochimiques) pourraient être imputée à la faible durée et la faible amplitude des émergences, un climat aride à semi-aride et une minéralogie originale dominée par la calcite faiblement magnésienne, paramètres ayant limité la

dissolution et le développement de produits diagénétiques vadoses. Un nouveau découpage séquentiel pour la Formation des Calcaires à Alvéolines est enfin proposé et discuté.

1 Introduction

5 Several authors have recently given new insights to an old problem: identification and
hierarchy of sedimentary discontinuities [Clari *et al.*, 1998; Hillgärtner, 1998;
Immenhauser *et al.*, 2000; Sattler *et al.*, 2005; Christ *et al.*, 2012a, 2012b, Hamon *et al.*,
2013]. Sedimentary discontinuities are often important marker horizons that represent basic
but essential features for sequence stratigraphy and paleoenvironmental reconstruction.
10 However, their recognition in the sedimentary record, specifically in shallow-water
carbonates may be difficult due to the variety of factors that may control their expression:
hiatus duration, climate, original carbonate mineralogy and texture of the underlying facies.
Moreover, these carbonate deposits are often affected by a strong burial diagenetic overprint
that may hinder the original sedimentary and geochemical signal [Joachimsky, 1994; Clari *et*
15 *al.*, 1998; Moore, 2001; Christ, 2012b].

In the Graus-Tremp Basin, despite its name, the Early Ilerdian (early Eocene) *Alveolina*
Limestone Formation is clearly a mixed carbonate-siliciclastic series, composed of bioclastic,
bioconstructed and siliciclastic facies, showing a large diversity of facies and complex
sedimentary architectures. The *Alveolina Limestone* Fm. has been extensively studied for
20 microfacies characterization and its use for paleoclimate assessment or biostratigraphic
purposes [Molina *et al.*, 2003; Rasser *et al.*, 2005; Scheibner *et al.*, 2007; Pujalte *et al.*, 2009].
Local-scale [Remacha and Zamorano, 1989; Payros *et al.*, 2000] and regional-scale works on
the sequence stratigraphy and stratigraphic architecture also exist [Eichenseer, 1988,

Eichenseer and Luterbacher, 1992; Leturcq, 1999; Baceta *et al.*, 2011]. Some significant differences (boundary's stratigraphic position, sequence types) exist between these works, that may be explain (at least partly) by the apparent lack of well-expressed sedimentary discontinuities and more specifically of exposure surfaces.

5 Based on spectacular outcropping conditions in the Serraduy area (located in the North-Western part of the Graus-Tremp Basin), this paper proposes an integrated approach, that aims at (1) describing the sedimentary facies and local architectures; (2) comparing these results with geochemical analyses (C and O isotopes and element geochemistry) performed on samples covering the whole stratigraphic interval; (3) using these combined dataset to identify
10 and hierarchize the different sedimentary discontinuities, and to discuss the puzzling absence of typical subaerial exposure-related criteria.

Geological setting

The study area (named Serraduy) is located in the Graus-Tremp Basin (Huesca Province), in
15 the southern flank of the Spanish Pyrenees. This basin makes up the easternmost part of the South Central Pyrenean unit [Séguret, 1972; Mutti *et al.*, 1988]. The latter corresponds to a set of allochthonous thrust sheets implying Mesozoic strata and Tertiary cover developed in piggyback sequences [Choukroune *et al.*, 1968; Séguret, 1972; Ori and Friend, 1984; Munoz, 1992]. During the last Oligocene sequence, the South Pyrenean Zone has been thrust over
20 the present autochthonous Ebro Foreland Basin. The sedimentary cover shows: 1) Mesozoic (Jurassic to Late Cretaceous-Coniacian) pre-orogenic marine carbonates; and 2) a Santonian to Early Miocene, syn-orogenic succession that shows deposits from turbidites to alluvial environments.

The sedimentary basins in the South Pyrenean Central Unit are bounded by three major thrusts rooted in the Triassic evaporitic decollement level: Boixols, Montsec, Sierras Marginales (Fig. 1A). The northernmost Boixols Thrust that corresponds to the Northern limit of the Graus-Tremp Basin was generated by the inversion of pre-existing E-W normal faults [Roure et al., 1989] during the Late Cretaceous (Santonian), and sealed by the Aren Sandstones (Maastrichtian age). Southward, the Montsec Thrust was active during Early Eocene (Ypresian age), and corresponds to the limit between the Southern part of the Graus-Tremp Basin, and the Ager Basin. The Sierra Marginales thrust makes the boundary between the Ager Basin and the present-day Ebro foreland basin, and was active from Mid-Eocene to Oligocene. During Ypresian times, the Graus-Tremp basin was an E-W elongated basin controlled southward by the active Montsec Thrust.

In terms of palaeogeography during Palaeocene-Eocene times, the Graus-Tremp Basin is part of an elongated gulf opened westward into the Bay of Biscay, bordering the axial zone of the Pyrenees to the North, and located at paleolatitudes between 35° and 38° [Butterlin *et al.*, 1993; Hay *et al.*, 1999]. The climate system is mainly characterized by warm, generally ice-free conditions, culminating into the Early Eocene Climatic Optimum around 53,5 Ma (EECO; Sloan and Thomas [1998]; Zachos *et al.* [2001]). Interspersed through this warm interval were a series of dramatic events in surface temperature, called hyperthermals, lasting tens of thousands of years, followed by rapid declines towards baseline warming rates. The most prominent one is the Paleocene–Eocene Thermal Maximum (PETM, around 55.8 Ma), characterized in the Pyrenees by a temperature rise and an increase in seasonal rain and intra-annual humidity gradient [Schmitz and Pujalte, 2007]. The studied interval takes place just after this PETM event.

The studied *Alveolina Limestone* Formation is part of the Early Tertiary fill of the basin (Figs. 1B and 2), characterized by the alternation of carbonate and siliciclastic facies. Late

Palaeocene deposits are formed of continental or brackish-water series belonging to the Tremp Formation [Mey *et al.*, 1968], passing westwards to shallow-water platform carbonates of the Navarri Formation [Garrido-Megias and Rios, 1972]. These formations are coeval with the end of the southward displacement of the innermost tectonic unit (Boixols), which itself is capped by later Eocene deposits. A renewed marine incursion took place in the South Pyrenean Gulf at the beginning of the Eocene (Lower Ilerdian, 56-55 Ma), with the shallow-water and reefal carbonate deposits of the *Alveolina Limestone* Formation [Nijman and Nio, 1975; this study]. These deposits are onlapping from the south onto the continental deposits of the Tremp Formation [Fonnesu, 1984]. At that time, the central tectonic unit of Montsec also began to move southwards. Middle and Late Ilerdian times are characterized by the sedimentation of the Riguala Marls [Tosquella, 1988], passing upward into the La Puebla Limestone Formation [Cuevas-Gozalo *et al.*, 1985] corresponding to a series of marly limestones, deposited in a shallow shelf environment. The overlying Roda Sandstone Formation (late Ilerdian to Cuisian; Cuevas-Gozalo *et al.* [1985]) is made up of six prograding sand bodies which are interbedded with nummulitic marls [Crumeyroille *et al.*, 1992]. The uppermost part of the Roda Sandstone unit is characterized by a transgressive sequence composed of marl/limestone beds (Morillo Limestone Formation; Cuevas-Gozalo *et al.* [1985]).

The studied *Alveolina Limestone* Formation covers two distinct *Alveolina* biozones [Hottinger, 1960; Serra-Kiel *et al.*, 1994] (Fig. 2): *Alveolina cucumiformis* (SBZ5; Gradstein *et al.* [2004]) and *Alveolina ellipsoidal* (SBZ6; Gradstein *et al.* [2004]). This formation is attributed to the Lower Ilerdian period [Payros *et al.*, 2000; Molina *et al.*, 2003].

Material and methods

The studied area is a square of 3 km by 3 km, centered on the village of Serraduy del Pon. The studied *Alveolina Limestone* Formation is cropping out in several well-exposed cliffs. Ten detailed sedimentological sections were described at the 1/100 scale (see Fig. 1C for location).

Petrographic analyses were carried out on 155 thin sections, with a Nikon Eclipse LV100 POL microscope. All thin sections have been stained with alizarin red-S to differentiate carbonate minerals (aragonite, calcite are stained, while dolomite remains unstained; Dickson [1966]) and potassium ferricyanide for distribution of ferrous iron. In order to estimate the amount of the different allochems, point counting on scanned thin sections has been performed, using JmicroVision Image analysis system [Roduit, 2008]. The point counting was performed using a random selection of points, and stopped based on a stochastic criterion (when the percentages are getting stable, the counting can be stopped). Oxygen (O) and carbon (C) isotope analysis have been performed on 84 samples, distributed over three representative sections of the Serraduy area (sections AB, H, N). Samples consists in larger-foraminiferas (*Alveolina* and *Nummulites*), apart for facies in which they are absent (facies B1, B2 and B3). In the latter case, samples correspond to bulk, dominated by Microcodium debris. Analyses were made at the Institute of Geology and Mineralogy of Erlangen (Germany) with the following procedure. Carbonate powders were reacted with 100% phosphoric acid (density >1.9, Wachter and Hayes [1985]) at 75°C using a Kiel III online carbonate preparation line connected to a ThermoFinnigan 252 mass-spectrometer. All values are reported in per mil relative to V-PDB by assigning a $\delta^{13}\text{C}$ value of +1.95‰ and a $\delta^{18}\text{O}$ value of -2.20‰ to NBS19. Reproducibility was checked by replicate analyses of laboratory standards and is better than $\pm 0,02$ (1σ).

Major, minor and trace element analyses have been performed for section N and composite section AB (64 samples). As sample splits of 0.25 and 0.5 g are required for this kind of analyses, sampling was performed on bulk matrix. Analyses were made at the Centre SPIN (Ecole Nationale Supérieure des Mines de Saint- Etienne) with the following procedure. The analyses were made by Inductively Coupled Plasma Emission Spectrometry (ICP-AES) after HF digestion for major and minor elements but Si, and selected trace elements (Sc, V, Zn, Sr, Y, Ba). A subset of the samples, only from section AB, was further analyzed for major elements by X-rays Fluorescence on glass beads to measure SiO₂ contents. Both analytical procedures were calibrated against international geostandards, and analytical accuracy is estimated in the 5% range. A multivariate statistical analysis has been performed on this dataset. A Principal Component Analysis (PCA) was carried out on the measured variables using their correlation matrix (Wold et al. [1987]) for a complete description of this method). Secondly an Agglomerative Hierarchical Clustering (AHC) was performed to help classifying our analyses into hierarchical clusters [Kaufman & Rousseeuw, 1990]. Statistical analyses were performed with the software XLStat.

Facies analysis

Nineteen sedimentary facies were defined by their texture, their constituents, their sedimentary structures, their fossils and/or trace fossils (when present). Several papers already described and interpreted similar macro- and microfacies in and outside the studied area [Plaziat, 1975; Plaziat, 1984; Eichenseer, 1989; Eichenseer and Luterbacher, 1992; Payros *et al.*, 2000; Rasser *et al.*, 2005; Scheibner *et al.*, 2007]. These facies were grouped into six facies associations, defined and then attributed to a specific depositional environment on the basis of their constituent facies, their vertical stacking, their lateral facies change and their

overall geometry [Wilson, 1975; Purser, 1980; Scholle *et al.*, 1983; Tucker and Wright, 1992]. As this Ilerdian interval is dominated by larger foraminifera (*Alveolina*, *Orbitolites*, *Nummulites*, *Assilina*...), we also used the analyses of Hottinger [1997], Geel [2000] and Rasser *et al.* [2005] to arrange the depth zonation of the larger-foraminifera facies. The facies
5 are detailed and interpreted in the following part.

Facies association A: Coastal plain

Description

This facies association is composed of four facies. Facies A1 is a reddish, polygenic,
10 heterometric and azoic clast-supported conglomerate, with a medium to coarse-grained sandstone matrix (Fig. 3A). It forms metre to plurimetre-thick erosive, fining-upward sheets, filling wide and low-relief scours (15-20m wide, for 1-2 m deep). This facies often exhibits trough-cross bedding associated to megaripples migrating toward the South-West. This facies is generally overlain by the facies A2, a fine- to medium-sandstones, with Miliolids and rare
15 bioclasts. It consists in decimeter-thick beds with trough-cross bedding and planar laminations. Facies A3 is composed of laminated, grey to reddish marly siltstones, with decimeter-thick level with abundant root traces and whitish carbonate concretions. Finally, facies A4 is a silty limestone facies, characterized by a wackestone texture with abundant small Miliolids, rare ostracods, ostreid bioclasts and *Alveolina*.

20 Interpretation

The dominant siliciclastic sedimentation, the presence of root traces and, when present, the restricted character of the faunal content (ostreids, Miliolids) suggest very proximal, continental to littoral environments. Indeed, facies A1-A2 were interpreted as braided streams, part of wave-dominated braid deltas by Eichenseer and Luterbacher [1992] or as

representing the proximal parts of a fluvial megafan by Schmitz and Pujalte [2007]. The presence of Miliolids and rare ostreid fragments in the facies A2, indicates a littoral, restricted marine environment in which these braided stream prograded. The facies A3 may be interpreted as coastal plain deposits, as indicated by the planar lamination (suggesting low hydrodynamism regime and decantation process) and bioturbation [Reading, 1996]. Locally, the presence of root traces and carbonate concretions indicates episodic development of paleosoils. Finally, the presence of ostracods and small benthic Miliolids in the facies A4 are indicators of restricted marine conditions, possibly brackish marshes [Flügel, 2004; Rey and Bousquet, 1981].

10

Facies association B: Deltaic complex

Description

This facies association consists of four mixed sandy-carbonate facies. Facies B1 is a bioturbated (*Thalassinoides*) fine to medium-grained sandstone, often organized in low-angle inclined stratifications, forming lobate structures up to 10 m in thickness, with a sharp erosional base (Figs. 3B and 3C). The bioclastic fraction (between 20 to 40%) is composed of *Microcodium*, pelecypod, Miliolid debris, associated with micritic intraclasts (Fig. 4A and 4B). A micritic matrix is occasionally observed. Facies B2 is a clayey facies, interfingering with facies B1 in the periphery of the lobes, forming decimeter- to meter-scale alternations of marls and fine-grained sandstones (Fig. 3B and 3C). Lignite fragments and burrows (both horizontal and vertical) are frequently observed in these two facies. Often associated to the previous ones, the facies B3 is composed of a sandy and bioclastic limestone. It forms small-scale channel fills, that exhibit sigmoidal cross-stratifications with current ripples at their top. Bioclasts are highly fragmented and show a large diversity (Miliolids, *Nummulites*, rare

Alveolina, echinoid debris, pelecypods, gastropods and Dasycladacean stem fragments, Fig. 4C). Finally, facies B4 is a gastropod-dominated wackestone, with some plane-parallel beds and a slight nodular aspect. Dasycladacean stem fragments associated with many Miliolids and rare fragmented, and micritized *Alveolina* and *Orbitolites* are also observed (Fig. 4D).

5 Interpretation

The absence of any open marine organisms and the abundance of detrital quartz suggest sedimentation in a restricted and very proximal environment. The lobate geometry, the internal sigmoidal structures and the erosional base of facies B1, point to terminal lobes of a fluvial-dominated delta, supplied from the North by distributary channels [Middleton, 1991; Walker, 1992]. The stratigraphic relationships between facies B1 and B2 point to a lateral facies change. B2 is thus interpreted as fringing shaly deposits, immediately downstream of B1 [Rey and Bousquet, 1981]. However, the sigmoidal cross-stratification and the mixed sandy-bioclastic infill tend to indicate a reworking by tidal currents. Facies B3 is interpreted as distributary channels (channelized structures) supplying the B1-B2 lobes. Finally, the bioclasts' association observed in B4 (mainly monospecific gastropods and green algae), suggests deposition in a calm, restricted environment such as interdistributary restricted ponds or mudflats [Rey and Bousquet, 1981; Rasser *et al.*, 2005].

Facies association C: Shallow inner ramp

Description

This facies association is composed of three carbonate and one marly facies. Facies C1 is an *Alveolina* and *Orbitolites* dominated wackestone to packstone, showing a highly nodular bedding. Allochems are moderately fragmented, micritized, and dominated by *Alveolina* (80-90%), and a varying amount of *Orbitolites* (0-15%) (Fig. 4E). Miliolids, echinoid, green algae

debris, and a few micritic intraclasts are also observed (Fig. 3F). *Lucina* in living position are commonly found. Facies C2 is a marly dominated facies, closely interstratified with C1 facies. *Lucina*, ostreids and rare *Alveolina* can be observed. Facies C3 is made up of megaripples, with opposite current directions, filling large-scale channels. The microfacies is
5 a micro-grainstone dominated by micritic peloids and Miliolids, a few echinoid debris and rare micritized larger-foraminifera (Fig. 4F).

In the Serraduy area, a large erosive channelized structure crops out, filled by a submarine dune bedform characterized by large inclined stratifications, with a dominant current direction towards the East (facies C4; Figs. 3D and 3E). The latter is 300 m long and ranges from 2 to
10 15 m in height. It is composed of several accretionary units, separated by minor erosional surfaces and can be divided into two sub-facies: a grainstone characterized by moderately fragmented *Alveolina*, *Orbitolites* and red algae as the most prominent components; a well-sorted micro-grainstone, dominated by *Miliolids* (10-15%) and rounded micritized undetermined bioclasts and intraclasts (20-25%) (Fig. 4G).

15 **Interpretation**

The environmental interpretation of medium-grained Alveolinid-Soritid facies with nodular aspect is still controversial in Eocene ramps (low-energy beaches, sea grass-covered grain flats, shallow subtidal ramp; see Beavington-Penney and Racey, 2004 and references herein). The high abundance of *Orbitolites* in the facies C1 suggests a very proximal setting, in the
20 shallowest parts of carbonate platforms [Hottinger, 1997; Geel, 2000]. As suggested by Rasser et al [2005] or Eichenseer and Luterbacher [1992], this facies may represent a beach environment. The muddy texture of the facies, suggests low-energy beaches that may border a calm lagoonal environment, represented by C2 facies.

On the contrary, the grainy texture and the high fragmentation observed in the C3 facies point to high energy conditions. Erosive base and sedimentary structures are thought to be formed by the migration of 3D-megaripples localized in a tidal channel (two opposite current directions), cutting through the previously described inner platform facies. High content in Miliolids also suggests a proximal platform interior setting [Geel, 2000].

The facies C4 is interpreted as a large-scale channel filled by a prograding megadune, as it is confined and probably elongated within the channel [Olariu and al., 2012]. A tidal origin is proposed by Eichenseer [1988] and Eichenseer and Luterbacher [1992] on the basis of the channelized morphology, the geometry and orientation of the clinofolds that prograded eastwards. The dominance of *Alveolina*, *Orbitolites* and red algae suggests a deposition in the open waters of an inner- to mid-platform setting [Scheibner *et al.*, 2007]. This channel filled by tidal dunes prograding into a lagoonal environment suggest a tidal inlet.

Facies association D: Mid-ramp

15 Description

Two carbonate facies are described in this facies association: Facies D1 is a silty wackestone dominated by fragmented *Alveolina* but entire globose *Nummulites* (Fig. 4H), associated with ostreids (generally encrusting top of beds) and echinoid debris, lacking sedimentary structures. No peculiar changes in the size or morphology of the larger-benthic foraminifera was observed. Facies D2 is a silty, *Operculina*-rich wackestone (Fig. 4I), moderately bioturbated, without any sedimentary structures. This facies occurs rarely and is generally interstratified with Facies D1.

Interpretation

Facies D1 is characterized by the mixing of two types of larger-foraminifera, which suggest two different environments [Geel, 2000]. Rasser *et al.* [2005] observed a similar facies in the Ilerdian Minerve section (Southern France) and interpreted it as an offshore-transport of *Alveolina* (from proximal area) into a more open and distal environment (presence of *Nummulites*). Such a mixing may be indicative of a mid-ramp setting. Eocene nummulitic accumulations have been studied by Mateu-Vicens *et al.* [2012], who proposed a mass flow origin. In the facies D1, nummulites are mostly entire, with very few nummulithoclasts and no sedimentary structures are observed, which suggest in situ deposition. Globose *Nummulites* are generally associated with the basal part of the euphotic zone to the shallowest part of the mesophotic zone [Hottinger, 1997; Pomar, 2001, Pomar *et al.*, 2014]. Geel [2000] proposed a depth range of 10 to 30 m for small and medium-sized, lens-shaped *Nummulites* (euphotic zone of Pomar [2001]). Similarly, the faunal composition of D2 (dominance of *Operculina*) suggests a deposition in an open marine, mid-ramp setting [Hottinger, 1997; Scheibner *et al.*, 2007]. *Operculina* is thought to be less dependent on coralline algae symbionts for food, and is therefore inferred to have had a wider environmental range than the other Nummulitids, commonly associated to the mesophotic zone [Hottinger, 1997; Boudagher-Fadel, 2008]. Such conditions commonly correspond to a depth range of 40 to 80 m of water depth [Pomar, 2001] but they may also occur in dense seagrass meadows or in case of important turbidity [Pomar *et al.*, 2014]. The absence of miliolids or green algae fragments do not support such hypothesis for facies D2, that may be associated to the lower part of the mid-ramp.

Facies association E: Outer-ramp

Description

This association generally consists in weathered moderately bioturbated wackestone beds (E1), pluridecimetric in thickness, alternating with marly facies (E2). The wackestone beds are dominated by *Assilina*, and subordinate *Operculina*, *Nummulites*, echinoid and crinoid debris and frequent glauconite grains associated with a minor lithified top surface (Fig. 4J). Again, no peculiar changes in the size or morphology of the larger-benthic foraminifera was observed.

Interpretation

The presence of *Assilina* and *Operculina*, the muddy texture and the absence of inner-platform foraminifera point to a mesophotic to oligophotic outer-ramp environment, below the fair-weather wave base. The presence of crinoid debris (photo-independent biota) or Nautiloids (described by Leturcq [1999], not observed in this study) also supports such hypothesis. Finally, the alternation of marly and carbonate facies with the occurrence of early lithified and glauconitic surfaces also suggest a low production rate. This is consistent with the interpretation of Rasser *et al.* [2005], Scheibner *et al.*[2007] or Scheibner and Speijer [2008].

Facies association F: Reefal facies

Description

At different intervals of the Lower Ilerdian succession, coral-dominated build-ups (averaging hundred meters of lateral extent and less than ten meters in height) are organized into three

parts (Figs. 3F, 3G and 3H). The core (and base) of the build-up is generally dominated by metric alternations of C1 (*Alveolina* and *Orbitolites* wackestone / packstone) and F1 facies (*Alveolina* and coral-dominated wackestone). The latter shows decimetric egg-shaped coral "bushes" composed of bulbous, tabular corals (*Poritidae*) and red algae (Fig. 4K), in a surrounding matrix composed of C1 facies. Progressively, metric beds of facies F2 are observed and finally forms the upper part of the build-up. Facies F2 is a framestone composed of bulbous and tabular corals, red algae and a few occurrences of encrusting foraminifera *Solenomeris*, are observed. The edges of the build-ups may show lateral accretionary sets, made up of reworked bioconstructed-derived material (*s.s.*), mixing all the previously described facies.

A second type of reefal facies has been observed in Section N, forming metre-thick biostromes, lacking a rigid framework (Fig. 3H). It is composed of a bindstone (to framestone) mainly composed of bulbous *Solenomeris* (encrusting foraminifera, *Acervulinidae* group) associated with red algae, rare bioclasts (echinoids, lamellibranches) and a micritic matrix (facies F3; Fig. 4L).

Interpretation

The faunal content of F1 and F2 points to a reefal environment. Recently, Morsilli *et al.* [2012] and Pomar *et al.* [2014] demonstrated the existence of Late Eocene, coral-dominated build-ups, in relatively deep, mesophotic zone and relatively nutrient-rich water. These build-ups are characterized by non-framework corals, with sparse coral colonies in a bioclastic, muddy matrix. Corals are also associated with red algae, bryozoans, mesophotic large-benthic foraminifera, serpulids and sponges. Finally the build-ups are completely encased in clay.

In our case study, the main body of the build-ups is made of a coral-dominated frame-built reef, without any bryozoans or sponge and very rare fragments of serpulids. The associated

matrix is an *Alveolina* and *Orbitolites* wackestone to packstone. The presence of Soritids and the absence of mesophotic/mesotrophic larger-benthic foraminifera (*Nummulites*, *Operculina*...) in the matrix suggests that these build-ups developed in a shallow inner- (or mid-ramp) setting [Scheibner *et al.*, 2007; Morsilli *et al.*, 2012]. This seems to be confirmed by the build-up association with facies C1, rather than deep facies. The internal architecture of the build-ups (abundant association of red algae and pioneer forms of corals at the base versus a higher diversity of branching, bulbous and lamellar corals at the top) may therefore indicate an evolution from mesotrophic environmental conditions to more oligotrophic conditions, in the euphotic zone [Tucker and Wright, 1992; Wood, 1999]. The absence of a detritic fraction (silts or clay) also suggests such oligotrophic/euphotic conditions. Finally, these build-ups are constantly eroded and the reworked material is accumulated laterally. In the facies F3, the absence of diversified forms of corals and the abundance of *Solenomeris* (pioneer, tolerant bioconstructors) suggest less optimal ecological conditions that lead to the reduction of competition for substrate encrustation (decrease of light intensity and hydrodynamic energy). They generally extend into deeper water than coral reefs, even in turbid environments [Perrin, 1992; Bosellini and Papazoni, 2003]. This is confirmed by the presence of a micritic matrix, that may indicate a low-energy environment, probably more turbid (outer periphery of lagoon or external margin of carbonate platform for Plaziat and Perrin [1991]).

20 **Local sedimentary architectures and sequence stratigraphy**

In Serraduy, due to the good outcrop quality, the sedimentary architectures were directly assessed on the field, by following the main discontinuities (erosional surfaces, hardgrounds). Thus, a 3D model illustrating the general architecture of the *Alveolina Limestone* in the Serraduy area is proposed in Figure 5. These observations enable us to propose a synthetic

depositional profile (Fig. 6A) with a proximal deltaic system (Facies Associations A and B) prograding into an inner ramp setting (FA. C), passing downstream to a mid (FA. D and F) then outer ramp setting (FA. E), and to identify small-scale transgressive/regressive cycles [Embry, 1993]. A purely descriptive and time-independent nomenclature is applied to designate the different scales of sedimentary cycles described in this study. The finest elementary cycles are called generically “small-scale cycles” (sensu Strasser and Hillgärtner [1998]), bounded by sedimentary discontinuities: sharp changes of facies, hardgrounds, erosional truncations... (Fig. 6B).

The first small-scale cycle (Fig. 6B) is limited at its base by a major, low-relief erosive surface, correlated over the whole studied area (S0). It is overlain by some metre-thick sheets of conglomerates (facies A1), corresponding to the Claret Conglomerate [Baceta et al., 2011]. It is followed by bioclastic sandstones (facies A2), and bioturbated siltites (facies A3). Bioclastic shallow inner-ramp facies (A4 and C1) are onlapping over a ravinement surface, suggesting a transgressive trend. In the Northern part of the area (section N; Fig. 3H and 5), a coral-dominated build-up developed, interstratified with this shallow inner-ramp facies. It is composed of *Poritidae*, and red algae boundstones (facies F1 and F2) with facies C1 at the base, grading upward into coral-dominated boundstones (facies F2). This could suggest a progressive deepening and improvement of the ecological conditions associated to the end of the transgressive trend, followed by an increasing coral growth (that forms the bulk of the bioherm) during the highstand conditions [Wood, 1999; Schlager, 2005]. In the Southern part of the area (sections C and F; Fig. 5), the shallow inner-ramp facies (facies C1) are overlain by a highly bioturbated and glauconitic thin interval (40 cm) of facies D2, which may represent the maximum flooding of the cycle. The regressive part of the cycle is eroded by the unconformity S1.

The second small-scale cycle (Fig. 6B) is bounded at its base by the surface S1, an erosive angular unconformity forming a large-scale (100 m wide, 4-5 m thick) channelized unit (Fig. 3E and 5), filled by facies C3. The preservation of the tidal channel fill suggests a positive accommodation, related to a transgressive trend. Upon it, a complex deltaic system developed, composed of at least seven sandy lobes (facies B1-B2) (Fig. 3E and 5), supplied from the North by multiple distributary channels (facies B3). Their spatial distribution is partly governed by a prograding trend and partly by stratigraphic compensation processes (i.e. the lobes are emplaced in negative topography between the previous ones). This interval may correspond to the regressive part of the cycle.

10 The third small-scale cycle (Fig. 6B) is bounded at its base by the surface S2, corresponding to a deeply scoured channel (sections AB, C, F and I; Fig. 3D, 3E and 5). A large bioclastic tidal bar (facies C4), passing laterally to a marly, *Lucina*-rich facies (C2) filled this structure (section D). Outside of the channel, some shallow, inner-ramp facies (C1) are observed. The preservation of the tidal channel fills suggests a positive accommodation, until a maximum marked by the preservation of the topset in the uppermost part of the bar [Emery and Myers, 15 1996]. This level is successively overlain by facies C2 and C1 (lagoonal and low-energy beaches), pointing to a prograding trend, that ended by a new discontinuity (surface S3).

Subsequently, the fourth small-scale cycle (Fig. 6B) is characterized by the development of several build-ups (sections N, G and F; facies F1-F2) interfingered with inner- (facies C1) to mid-ramp facies (facies D1) (Fig. 3F, 3G and 5). This points to a general improvement of the ecological conditions of the depositional environment [Wood, 1999; Brock *et al.*, 2008], with a decrease of the detrital influx (confined to the most proximal regions) and an increase of the hydrodynamism associated to the transgressive phase of the cycle. The latter is followed by the outer-ramp facies (E1 and E2), and capped by mid-ramp facies (D1) which may point to a

new prograding trend. The fourth cycle ends with a mineralized and glauconite-rich surface (S4).

The fifth (and last) cycle (Fig. 6B) is composed at its base by outer-ramp facies (facies D2, E1, alternating with marly facies E2). In the Northern part of the area, a meter-scale *Solenomeris* reef-mounds is observed (facies F3) (section N; Fig. 3H and 5). The absence of corals and the large development of *Solenomeris* point to a deterioration of the ecological conditions, that could be linked to the stability of water masses during the end of the cycle [Lukasik and James, 2003]. The succession is topped by a mineralized and glauconite-rich surface, encrusted by *Solenomeris* and Bryozoans (surface S5).

At this step, due to the absence of clearly marked exposure criteria and the lack of unequivocal stacking pattern in this shallow ramp setting, it is difficult to hierarchize these small-scale cycles and to describe larger-scale trends. To overcome these problems, complementary geochemical analysis have been performed and are presented hereafter.

15 **Geochemistry**

Isotope geochemistry

The results of O and C isotope analyses for the Serraduy area (Table 1 – Supplementary Material) have been plotted in $\delta^{18}\text{O}$ versus $\delta^{13}\text{C}$ cross-plots (Fig. 7) and vertically along the sedimentary logs (Fig. 8). As a general point, these isotopic values are characterized by a good covariance between the $\delta^{18}\text{O}_{\text{V-PDB}}$ and $\delta^{13}\text{C}_{\text{V-PDB}}$ (Fig. 8) and possibly by the inverted J-shaped curve [Lohmann, 1988] (Fig. 7). Three fields of isotopic values can be distinguished.

A first field is characterized by isotopic values ranging from -4.10‰ to -2.37‰ for $\delta^{18}\text{O}_{\text{V-PDB}}$ and 1.12‰ to 2.59‰ for $\delta^{13}\text{C}_{\text{V-PDB}}$ (Fig. 7). They corresponds to larger-foraminifera samples and are spread in the cycles 1, 3, 4 and 5 (Fig. 8). The $\delta^{13}\text{C}_{\text{V-PDB}}$ values fall in the range of the

isotopic signatures of the Lower Eocene marine calcite from Veizer *et al.* [1999] (grey domain in Fig. 8), whereas the $\delta^{18}\text{O}_{\text{V-PDB}}$ values are shifted toward more negative signatures.

The second field of isotopic values is characterized by negative $\delta^{18}\text{O}_{\text{V-PDB}}$ values (-4.19‰ to -3.12‰) and slightly negative to positive $\delta^{13}\text{C}_{\text{V-PDB}}$ (-1.69‰ to 1.28‰) (Fig. 7). These samples also correspond to larger-foraminifera, but are located below peculiar sedimentary discontinuities. Thus, discontinuities S1 and S3 are marked by a slight shift toward $\delta^{13}\text{C}_{\text{V-PDB}}$ negative values in section N (Fig. 8). This slight but sharp decline is only observed below S3 in the other studied section (AB and H). Apart from this slight negative shift in the vicinity of bounding discontinuities, no specific vertical variations are observed along one single cycle (Fig. 8).

Finally, the third field of data displays strongly negative values, both in $\delta^{18}\text{O}_{\text{V-PDB}}$ (-6.68‰ to -4.91‰) and in $\delta^{13}\text{C}_{\text{V-PDB}}$ (-6.41‰ to -4.08‰) (Fig. 7). These samples are located in the siliciclastic-dominated interval (cycle 2; Fig. 8), where the carbonate fraction mainly corresponds to *Microcodium* debris.

Elemental geochemistry

The results of the elemental values for the Serraduy area (Table 1 – Supplementary Material) have been analysed through a multivariate statistical analysis: the Principal Component Analysis (PCA). PCA is broadly used in geochemical studies [Azevedo *et al.*, 2008; Marques *et al.*, 2008 and reference herein]. In the case of a geochemical data matrix, each vector shows that the data spread according to their geochemical affinity and provenance. A first PCA was done on the whole dataset (Figs. 9A and 9B), excluding the Si variable, as Si analyses were carried out only on a subset of samples, from section AB. A second PCA was then performed on this specific subset, including all the variables (Fig. 9C).

The PCA (Fig. 9) and their associated Pearson correlation matrix (Table 2) show several relationships between key parameters. In the first PCA (Fig. 9A; Table 2A), several strong positive correlations are highlighted, such as Al_2O_3 with TiO_2 , Na_2O and K_2O . In the PCA circle of correlation (Fig. 9A), these positively correlated variables tend to be close. Moreover, the second PCA (Fig. 9C; Table 2B) shows that these variables are also strongly correlated with Si_2O . Negative correlations between CaO and these variables (Al_2O_3 , TiO_2 , Na_2O and K_2O) are observed in the PCA circle of correlation, where negatively correlated variables tend to be diametrically opposed in the projections (Fig. 9A; Table 2A). Finally, Fe_2O_3 and MnO are significantly negatively correlated with CaO , whereas MgO and SrO are not correlated with Ca . On the other hand, Fe_2O_3 , MnO and MgO seems partly correlated with Al and Si (and the abundance of siliciclastics).

These latter correlations can also be illustrated by the vertical plots of elemental contents along the sedimentary logs of sections AB and N (Fig. 10). The analysed samples are characterized by moderate to low content of Mg , mainly ranging from 5500 to 9500 ppm in both sections (Fig. 10). The Mg/Ca molar ratio calculated for carbonate samples (Table 1 – Supplementary Material) are typical of low- Mg calcites [Carpenter and Lohmann, 1992; Sherman et al., 1999]. Fe_2O_3 vary from 0 to 5700 ppm in section N and from 400 to 7700 ppm in section AB with the same trends and positive anomalies (up to 21000 ppm) than for Mg . A slight enrichment both in Mg and Fe is observed in the siliciclastic-dominated facies (facies B1 to B4) of cycles 2 and 3 (Fig. 10), which could be explained by several hypothesis: presence of biotite, and presence of small dolostone clasts coming from reworked layers of Garumnian Fm. deposits (not observed in the studied thin section). In section AB, a few positive anomalies (up to 15000 ppm) are observed, corresponding to basal lags just above erosive surfaces (S1 and S2; Fig. 10).

MnO content is relatively similar in the two studied sections (Fig. 10). It is low to moderate, varying from 50 to 250 ppm in carbonate facies, and from 300 to 800 ppm in siliciclastic-dominated facies. No peculiar relationship with stratigraphic surfaces is observed (Fig. 10). However, they are clear sequence-related differences : a substantial MnO enrichment is observed in the siliciclastic-dominated facies of the cycles 2 and 3 (Fig. 10). It may be related to the abundance of soil-derived particles (Krumbein and Jens, 1981; Woody et al., 2014) or eventually to *Microcodium* clasts (Kosir, 2004).

SrO content exhibits low and slightly fluctuating values (mean 672 and 750 ppm, respectively in sections N and AB; Fig. 10). The siliciclastic-dominated facies display the lowest values (Fig. 10). SrO content of the carbonate facies is characterized by significantly lower values in cycle 1, compared to cycles 3, 4 and 5. These values are in line with those of low-Mg calcites [Carpenter and Lohmann, 1992; Sherman et al., 1999].

Finally, the large majority of the analyzed samples shows low Na contents. The latter are more important in siliciclastic-dominated facies (300 to 1100 ppm) than in carbonate ones (150 to 400 ppm). Higher values are observed in carbonates at the base of section N, ranging between 600 to 900 ppm. A shift toward minimum values is observed below the surface S1 in section N and below S3 in both sections (Fig. 10).

Cluster analysis

The PCA carried out previously also enables us to look at the data on a two-dimensional map and to identify trends, through a proximity analysis of the different points (Fig. 9B). On this figure, a dense cloud of points is observed near the center of the circle. It is composed of carbonate-dominated samples, including the samples located below discontinuities S1 and S3. A second group of points may be observed, corresponding to the siliciclastic-dominated samples (facies B1, B3 and B4). Finally, a few atypical points are scattered away from these

groups (C9, C11, N1, N20 and B9) and correspond to lag deposits, situated just above erosional surfaces.

The interpretation of the dense point cloud directly on the PCA circle may be tricky as the points situated near the circle center are generally badly represented in the factors space (Fig. 9B). An Agglomerative Hierarchical Clustering (AHC) was therefore performed to help classifying these specific analyses (carbonate-dominated samples, excluding the siliciclastic-dominated samples) into hierarchical clusters. The AHC works from the dissimilarities between the objects to be grouped together. The results are illustrated in the dendrogram of Fig. 10, wherein the cluster distance on the vertical axis represents the level of association between groups of observations (data); short distance values indicate the greatest similarity between variables. Three groups may be isolated. The first (green color) group is made of samples of lag deposits (C9, N1 and B9) and is more heterogeneous than the other ones (within-class variance a lot higher for the first group). The samples PA1 and B2 were not identified in the PCA circle but correspond to the very base of carbonate beds and may be associated to lag deposits. The third group (blue color) corresponds to the major part of the carbonate samples, whereas the second group (purple color) is composed of carbonate samples located in the vicinity of discontinuities S1 (samples N10, N12, N13, N14) and S3 (samples B22, B23, B24, N23, N24). Samples N3 and N8 are located in the cycle 1 (facies F1 and F2), whereas the sample N19 corresponds to B4 facies in cycle 3. The origin of this clustering will be discussed in the following part of the article with also the specificity of sample C11 that appears as a single value (in black).

Discussion

Insight from isotope geochemistry

The isotopic values in the Serraduy succession are in the same range than those in the Upper Paleocene - Lower Eocene limestones in the Ermua and Zumaya sections (Basque Country, Northern Spain; Schmitz *et al.* [1997]), in the Esplugafreda section (Graus-Tremp Basin; Schmitz *et al.* [1997]; Schmitz and Pujalte [2003]) or in the Campo section [Molina *et al.*, 2003]. These previous isotopic studies have shown that the whole rock samples of limestone and calcite-rich marls give reliable $\delta^{13}\text{C}$ results. In our case study, apart from the samples taken in the siliciclastic-dominated interval, the isotopic data comes from analyses of *Alveolina* and a few *Nummulites*. These two genus are both epifaunal and may spanned in nearly comparable paleoenvironments (lagoon to mid-shelf, warm, normal marine water; Boudagher-Fadel, 2008). This similarities may prevent a significant differential fractionation due to the vital effect of these benthic larger-foraminiferas (Schmiedl *et al.*, 2004; Friedrich *et al.*, 2006). This seems to be confirmed by the $\delta^{18}\text{O}$ versus $\delta^{13}\text{C}$ cross-plots where the values of both type of samples fall in the same range of values (first field of values, Fig. 7). The isotopic variations observed between the different field of values may therefore be considered as diagenetic rather than original.

As it was presented previously, three field of isotopic values have been identified. The first and main one shows $\delta^{13}\text{C}_{\text{V-PDB}}$ values in the range of the Lower Eocene marine calcite from Veizer *et al.* [1999], which is in line with the marine nature of these deposits and the apparent absence of meteoric / continental alteration. The $\delta^{18}\text{O}$ signatures are shifted toward negative values from 1 to 3‰, compared to the isotopic signatures of the Lower Eocene marine calcite from Veizer *et al.* [1999]. Such values may suggests the recrystallization of the foraminifera tests and a thermal fractionation of the oxygen isotopes associated to a gradual increase of temperature during burial. The preservation of the $\delta^{13}\text{C}$ original signal could be explained by

the fact that these sediments were indurated or compacted during early diagenesis and may represent relatively closed systems with respect to carbon isotopes [Molina *et al.*, 2003].

The second field of values, is composed by samples taken below discontinuities S1 and S3.

These boundaries are both marked by depleted $\delta^{13}\text{C}_{\text{V-PDB}}$ signatures (-1 to +0.5‰) compared

5 to marine calcite values (+1.5 to +2.5‰) and by a slight shift toward lower $\delta^{18}\text{O}_{\text{V-PDB}}$ values.

The $\delta^{13}\text{C}_{\text{V-PDB}}$ signatures are relatively high values to support precipitation or recrystallization from a meteoric fluid that are generally associated to a strongly negative carbon isotopic

composition [Allan and Matthews, 1982; Quinn, 1991]. However, the $\delta^{13}\text{C}_{\text{V-PDB}}$ signal of the

abundant marine calcite in the sediments may have overprint signals from any meteoric

10 carbonate that possibly precipitated in pores during early meteoric diagenesis associated to

exposure [Dickson and Saller, 1995; Moore, 2001]. The recrystallization of foraminifera or a

meteoric cement precipitation in the foraminifera chambers, mixed during sampling may

explain such $\delta^{13}\text{C}_{\text{V-PDB}}$ values. The slight depletion of $\delta^{18}\text{O}_{\text{V-PDB}}$ values observed below the

surfaces is more difficult to interpret. Such a shift is often associated with the signal of

15 isotopically light meteoric oxygen, but the $\delta^{18}\text{O}_{\text{V-PDB}}$ seems hardly reliable (possible thermal

fractionation during burial). This may be confirmed by the covariant trend (inverted J-shaped

curve) between $\delta^{18}\text{O}$ and $\delta^{13}\text{C}$ values, which suggest progressive diagenesis under meteoric

water conditions [Lohmann, 1988].

Finally, the last field of isotopic values is characterized by strongly negative values, both in

20 $\delta^{18}\text{O}_{\text{V-PDB}}$ and in $\delta^{13}\text{C}_{\text{V-PDB}}$. These samples are located in the siliciclastic-dominated interval,

where the carbonate fraction mainly corresponds to reworked *Microcodium* debris. Such

values are common in biogenic calcrete dominated by such allochems [Kabanov *et al.*, 2008;

Brlek and Glumack, 2014]. They are interpreted to have formed in isotopic equilibrium with

soil CO₂, which derives mainly from root respiration and microbial decomposition of soil

25 organic matter [Cerling, 1984; Brlek and Glumack, 2014]. The oxygen isotope composition of

calcretes is also directly related to that of the meteoric (rainfall) water from which they formed, with some alteration caused by selective infiltration and evaporation (Alonso-Zarza, 2003). Such values points toward arid conditions with ephemeral heavy rainfall, characterizing the depositional period (Thanetian) of the Garumnian series [Schmitz and Pujalte, 2003 and 2007]. These Garumnian deposits are eroded and reworked in deltaic facies during Ilerdian times.

Insight from elemental geochemistry

The multivariate statistical analysis (PCA and ACH) carried out previously have enable to group samples that share comparable geochemical signatures. The PCA show strong positive correlations between Al_2O_3 with Si_2O , TiO_2 , Na_2O and K_2O . These signatures are characteristic of siliciclastic-dominated samples. Indeed, these correlation are indicative of a terrigenous fraction mainly formed by quartz, clay minerals, calco-sodic- and K-feldspar, and disperse muscovite, which is in line with the petrographic observations. The co-variation between SiO_2 and Al_2O_3 , in particular, reflects the partition of Si between quartz and aluminosilicate minerals. Strong correlation between Al_2O_3 with K_2O on the one hand, and SiO_2 with K_2O on the other hand confirm the presence of significant amounts of K-feldspar in the terrigenous fraction [Lentz, 2003; Sageman and Lyons, 2003; Madhavaraju, 2015]. Similarly, the correlation between Al_2O_3 , SiO_2 and TiO_2 , probably highlights the presence of a heavy mineral contribution together with the siliciclastic input.

Negative correlations between CaO and these variables (Al_2O_3 , TiO_2 , Na_2O and K_2O), obviously reflects the distribution of silicate-bound elements in the siliciclastic samples versus the Ca-rich carbonate samples. It is generally considered that Ca, Mg, Sr, Fe and Mn contents are relevant to the interpretation of carbonate sedimentology and diagenesis [Graf, 1960; Morse, 2003]. The CAH realized on these carbonate-dominated samples enables to

identify three main groups: samples taken in the vicinity of discontinuities S1 and S3; samples corresponding to basal lag deposits; other carbonate samples, without any peculiar stratigraphic distribution.

Samples located below discontinuities S1 and S3 are characterized by minimum contents in MgO, Fe₂O₃ and MnO. The decreasing values in MgO may indicate a dominant recrystallization of aragonitic or HMC allochems in a low-Mg calcite, that may have operate under oxidizing conditions as these calcites are also characterized by a minimum content in Fe and Mn [Webb *et al.*, 2009; Tucker and Wright, 1992]. These geochemical data are consistent with an early meteoric diagenesis, associated to exposure [Moore, 2001]. The SrO content do not show such deviation in the vicinity of S1 and S3. The low SrO content observed in the first cycle, compared to the rest of the succession may eventually suggest partial leaching and/or recrystallization due to meteoric diagenesis, associated with the discontinuity S1. However, the original low-magnesian calcite composition of these carbonates (calcite sea period; Hardie, 1996), originally low in SrO, may have also masked the depletion in SrO classically associated to meteoric diagenesis [Moore, 2001], thus explaining the absence of peculiar Sr signature below these surfaces. Finally, the large majority of the analyzed samples shows probably too low Na contents to show good correlation with Ca in the PCA. In the carbonate facies, Na could reflect the presence of fluid inclusions (NaCl type) in the calcite crystals or at grain boundaries, being electrically incompatible with the calcite lattice [Gasse *et al.*, 1987].

A few samples shows anomalic values compared to the large majorities of the carbonate samples. Contents in Al₂O₃, MgO or Fe₂O₃ may display values five to ten times higher than the values of normal carbonates. In a lesser extent, MnO and TiO₂ may also show minor shift toward higher values. These samples are rich in glauconite grains and glauconized Miliolid tests, which could explain such enrichments. The enrichments in Fe₂O₃, MnO and TiO₂ may

also be related to the abundance of soil-derived particles, such as oxides and hydroxides. The enrichment in SrO content of facies C11 (4567 ppm) may be due to the presence of reworked aragonitic allochems such as coral debris.

5 Hierarchization of the stratigraphic surfaces

In Serraduy, six major stratigraphic discontinuities (named S0 to S5) can be recognized in the studied interval. Their characterization and interpretation are difficult due to the apparent absence of erosional features or diagnostic elements of exposure. Indeed, no epikarst features, typical vadose diagenetic products or in situ *Microcodium* (a distinct and widespread feature
10 in the whole Paleogene of the Pyrenees; Scheibner *et al.* [2007]) are observed. This observation can be generalized to other areas of the Graus-Tremp basin: on the Campo section, Payros *et al.* [2000] also conclude on the difficulty to identify stratigraphic sequences as none of the sequence bounding surfaces show evidence of subaerial exposure. However the approach developed in this study may help to characterize and hierarchize them.

15 The first surface (S0) corresponds to a major erosional surface, at the base of a 2m-thick, isopachous bed of polygenic and heterometric conglomerate (“Claret Conglomerate”). It was considered by Eichenseer and Luterbacher [1992] as a major incision (incised valley fill) and the basal sequence boundary of the so-called “Serraduy sequence” (Fig. 12). On the Campo section (reference section for the Ilerdian stage, situated 15 km W-NW of Serraduy), it
20 corresponds to a *Microcodium*-bearing surface, with karstic features [Payros *et al.*, 2000; Scheibner *et al.*, 2007]. Our geochemical dataset do not cover the base of the section. However, according to the latest isotopic studies by Schmitz and Pujalte [2003], the Surface S0 could correspond to the newly defined Paleocene/Eocene boundary and is considered as a major sequence boundary.

Surfaces S1 and S3 show interesting similarities. In the Northern part of the area, S1 is a slightly erosive surface, with apparent conformity and selective dissolution. A moderate moldic porosity is observed below the discontinuity, resulting from the dissolution of aragonitic coral debris and gastropods. In the Southern part of the area, S1 corresponds to an angular unconformity. S3 is a planar, very regular, mineralized surface (iron oxides and hydroxides and glauconite grains). A significant moldic porosity is also observed below the discontinuity, which suggests undersaturation of the diagenetic fluids with respect to aragonite, possibly meteoric fluids. The geochemical trends described above, both in terms of elemental and isotope geochemistry, are also indicative of such a meteoric diagenesis. The absence of any diagenetic or geochemical trend below S1 in section AB may be explained by an erosive character of the unconformity. S1 reflects exposure conditions, resulting of an eustatic drop combined with a significant tectonic activity (angular unconformity). Indeed, a significant syn-sedimentary tectonism during the deposition of the *Alveolina Limestone* Fm. is described in the form of a slow progressive flexuring of the basin floor due to the emplacement of a basal thrust sheet (referred in the regional nomenclature as Montsec thrust; Eichenseer and Luterbacher [1992]; Lopez-Blanco *et al.* [2003]). S3 also reflects subaerial exposure and is thus considered as a sequence boundary (Fig. 12). However, it only represents a low-amplitude sea-level drop (probably eustatic) without any significant tectonic. It is therefore less clearly expressed than S1, with no erosional feature or angular unconformity. The absence of sedimentary criteria of exposure may be explained by their erosion during exposure and the subsequent transgressive trend [Durllet and Loreau, 1996; Hamon *et al.*, 2013]. More broadly, the global greenhouse context during the Paleogene period, may have led to short-term subaerial exposures, precluding the development and preservation of widespread vadose diagenetic products [Read, 1998; Pomoni-Papaioannou and Kostopoulou, 2010]. The subtropical but semi-arid to arid climate is also in agreement with a limited degree

of meteoric alteration [Moore, 2001, Christ *et al.*, 2012a]. Finally, it is important to note that most of the studied unit is composed of carbonates of original low-magnesian calcite composition (calcite sea period; Hardie, 1996), thus prone to limited leaching and dissolution by meteoric fluids during exposure.

5 At the scale of the studied area, S2 is an erosional surface (channel), whereas S4 is a glauconite-rich firmground. Surfaces S2 and S4 do not show any deviation of the isotopic curves as for S1 and S3. The isotopic analyses fall in the main field of values. Surface S2 is characterized by a sharp positive shift in most of the analyzed elements, which have been interpreted previously as representing a lag deposits, just above erosional surfaces. S4 lacks
10 this peculiar geochemical trend and is characterized by values typical of silty carbonates. These two surfaces are not recognized by any author [Eichenseer and Luterbacher, 1992; Payros *et al.*, 2000]. Regionally, these surfaces are not easily correlatable. The absence of marked diagenetic alteration and geochemical trends suggests that these surfaces are not linked to exposure events. As a consequence, we consider them as local surfaces, with a
15 minor stratigraphic impact compared to S1 and S3 (Fig. 12).

Finally, in Serraduy, the last major discontinuity (surface S5) is a mineralized and glauconitic firmground, encrusted by *Solenomeris* and Bryozoans. For Eichenseer and Luterbacher [1992], it corresponds to a regional unconformity, bounding the Ager and Llimiana sequence (Fig. 12), and more generally, the *Alveolina Limestone Fm.* [Serra-Kiel *et al.*, 1994]. On the
20 Campo section, it consists in a sharp surface, between thinly stratified marly limestones and a mud-supported debris-flow, overlain by thin-bedded mixed siliciclastic-bioclastic turbidites [Payros *et al.*, 2000; Scheibner *et al.*, 2007]. This surface is interpreted as a maximum-regression-related surface, resulting in sea-floor omission and lithification [Christ *et al.*, 2012b].

7.4 A new sequence stratigraphy model for the *Alveolina* Limestone Fm.

Many sequence stratigraphic interpretations were already published for the studied stratigraphic interval in the present article. Some significant differences in both the number of sequences and the location of their bounding surfaces are easy to highlight between them (Fig. 12). The first and main works providing a detailed facies architecture and sequence arrangement of the *Alveolina* Limestone Fm. at Serraduy are those by Eichenseer [1989] and Eichenseer and Luterbacher [1992], who also studied this complex unit across most of the Tremp-Graus region of the southern Pyrenees. These authors described two third-order sequences, for the studied interval: the Serraduy and Ager sequences. Based on the sedimentological and biostratigraphic analysis of the Campo section, Payros *et al.* [2000] defined a new sequence stratigraphic interpretation that integrates three third-order sequences for the same stratigraphic interval: IL-1, approximately corresponding to the Serraduy sequence sensu Eichenseer [1989]; IL-2 and IL-3 corresponding to the whole Ager sequence sensu Eichenseer [1989] (Fig. 12).

Based on the stacking pattern and on the identification of the major stratigraphic discontinuities, we recognized three depositional sequences, each composed of one or several small-scale cycles. The first depositional sequence is bounded by surfaces S0 and S1. It is composed of the first small-scale sequence and is similar to the “Serraduy sequence” [Eichenseer and Luterbacher, 1992] and the IL-1 sequence of Payros *et al.* [2000].

Considering the unconformable character of the basal surface S0 and the prograding to aggrading geometry of the “Claret conglomerate” [Baceta *et al.*, 2011; Schmitz and Pujalte, 2007], these first deposits may be considered as a lowstand system tract. The floodplain clay preservation and the development of paleosoils suggest an aggradation context, consistent with a transgressive system tract. The slightly erosive contact between these deposits and the first *Alveolina* and *Orbitolites*-rich limestone may be considered as a marine ravinement

surface. Finally, the highstand deposits are absent or very limited in thickness, being eroded by the surface S1 (Fig. 12). The second and third depositional sequences are both composed of two small-scale cycles. The second depositional sequence is bounded by the surfaces S1 and S3 whereas the third one is limited by surfaces S3 and S5. They are equivalent to the unique Ager sequence of Eichenseer and Luterbacher [1992], but may correspond to the sequences IL-2 and IL-3 [Payros *et al.*, 2000], in terms of boundary location but also in terms of facies succession. In this framework, the second depositional sequence may be divided in a lowstand system tract (southward-prograding siliciclastic-dominated interval between S1 and S2), transgressive and highstand system tracts dominated by carbonate facies (Fig. 12). The third depositional sequence does not record such lowstand system tract, as it is emplaced in a general context of increasing accommodation. A major flooding thus occurs directly after surface S3, which also corresponds to a transgressive surface with development of reefal facies (Fig. 12). Giving the local scale of this study, this new sequence stratigraphy model needs to be tested to a more regional scale, which will be addressed in future works.

15

Conclusion

The multi-scale description of the facies and the geometries, combined with a detailed geochemical study of the *Alveolina Limestone* Formation in the Serraduy area (North of the Graus-Tremp Basin) illustrated the complexity of these Early Ilerdian series.

20 Classically, based on the facies identification and the sedimentary architectures description, it was possible to identify high-resolution T/R cycles. However, the cycle-bounding discontinuities lack typical exposure sedimentary criteria (no epikarst features, typical vadose diagenetic products or in situ *Microcodium*), which prevent the hierarchization of the cycle-bounding discontinuities and the recognition of larger-scale trends. This study demonstrated

that a detailed isotopic and elemental geochemistry study may complete adequately the sedimentological characterization by providing geochemical signatures to cycle bounding-discontinuities. In our case study, major discontinuities (angular unconformity, exposure surfaces) are characterized by a selective dissolution, a slight but sharp decrease in $\delta^{13}\text{C}_{\text{V-PDB}}$ and in Mg, Fe and Sr contents, below the surface. This hierarchization enables to recognize three depositional sequences, consistent with other recent regional studies. This study shows the pertinence of integrating sedimentological and geochemical studies, as a combined tool for sequence stratigraphy purposes.

Acknowledgements: The authors thank Pr. Michael Joachimsky at the University of Erlangen – Germany (Institute of Geology and Mineralogy), for performing the C and O stable isotopes analyses. The authors also thank Herman Ravelojaona (IFPEN) for thin sections preparation. The authors acknowledge the associate editor Pr. Pierre-Yves Collin and the reviewers Pr. Laurent Emmanuel and Dr. Philippe Léonide for their helpful comments that greatly improve this manuscript.

References

- ALLAN J.R. & MATTHEWS R.K. (1982). – Isotope signatures associated with early meteoric diagenesis. – *Sedimentology*, **29**, 797-817.
- ALONSO-ZARZA A.M. (2003). - Palaeoenvironmental significance of palustrine carbonates and calcretes in the geological record. – *Earth-Science Reviews*, **60**, 261-298.
- AZEVEDO D.A., TAMANQUEIRA J.B., DIAS J.C.M., CARMO A.P.B., LANDAU L. & GONCALVES F.T.T. (2008). Multivariate statistical analysis of diamondoid and biomarker data from Brazilian basin oil samples. - *Fuel*, **87**, 2122–2130.

- BACETA J.I., PUJALTE V., WRIGHT V.P. & SCHMITZ B. (2011). - Carbonate platform models, sea-level changes and extreme climatic events during the Paleocene-early Eocene greenhouse interval: a basin-platform-coastal plain transect across the southern Pyrenean basin. *In: C. ARENAS, L. POMAR and F. COLOMBO, Eds, Geo-Guías 7. Pre-Meeting Field trips. - 28th IAS Meeting, Zaragoza, 101-150.*
- 5
- BEAVINGTON-PENNEY S.J. & RACEY A. (2004). - Ecology of extant nummulitids and other larger benthic foraminifera: applications in palaeoenvironmental analysis. - *Earth-Science Reviews*, **67**, 219–265.
- BOSELLINI F.R. & PAPAZZONI C.A. (2003). - Palaeoecological significance of coral-encrusting foraminiferan associations: A case-study from the Upper Eocene of northern Italy. - *Acta Palaeontologica Polonica*, **48**, 279-292.
- 10
- BOUDAGHER-FADEL M.K. (2008). - Evolution and Geological Significance of Larger Benthic Foraminifera. - *Developments in Palaeontology & Stratigraphy*, vol. 21. Elsevier Publisher, 540 p.
- BRLEK M. & GLUMAC B. (2014). - Stable isotopic ($\delta^{13}\text{C}$ and $\delta^{18}\text{O}$) signatures of biogenic calcretes marking discontinuity surfaces: a case study from Upper Cretaceous carbonates of central Dalmatia and eastern Istria, Croatia. – *Facies*, **60**, 3, 773-788.
- 15
- BROCK J.C., PALASEANU-LOVEJOY M., WRIGHT C.W. & NAYEGANDHI A. (2008). - Patch-reef morphology as a proxy for Holocene sea-level variability, Northern Florida Keys, USA. - *Coral Reefs*, **27**, 555-568.
- 20
- BUTTERLIN J., VRIELYNCK B., BIGNOT G., CLERMONTÉ J., COLCHEN M., DERCOURT J., GUIRAUD R., POISSON A. & RICOU L.E. (1993). - Lutetian (46–40 Ma). *In: J. DERCOURT, L.E. RICOU and B. VRIELYNCK, Eds, Atlas of Tethys paleoenvironmental maps. - Paris, Gauthiers-Villars, 197–209.*

- CARPENTER S.J. & LOHMANN K.C. (1992). - Sr /Mg ratios of modern marine calcite: Empirical indicators of ocean chemistry and precipitation rate. – *Geochimica et Cosmochimica Acta*, **56**, 1837-1849.
- CERLING T.E. (1984). - The stable isotopic composition of modern soil carbonate and its relationship to climate. - *Earth and Planetary Science Letters*, **71**, 229– 240.
- CHOUKROUNE P., SEGURET M. & GALDEANO A. (1973). - Caractéristique et évolution structurale des Pyrénées: un modèle de relation entre zone orogénique et mouvement des plaques. – *Bulletin de la Société Géologique de France*, **15**, 600–611.
- CHRIST N., IMMENHAUSER A., AMOUR F., MUTTI M., PRESTON R., WHITAKER F.F., PETERHÄNSEL A., EGENHOFF S.O., DUNN P.A. & AGAR S.M. (2012a). - Triassic Latemar cycle tops: Subaerial exposure of platform carbonates under tropical arid climate. - *Sedimentary Geology*, **265–266**, 1–29.
- CHRIST N., IMMENHAUSER A., AMOUR F., MUTTI M., TOMAS S, AGAR S.M., ALWAY R. & KABIRI L. (2012b). - Characterization and interpretation of discontinuity surfaces in a Jurassic ramp setting (High Atlas, Morocco). - *Sedimentology*, **59**, 1, 249–290.
- CLARI P.A., DELLA PIERRE F. & MARTIRE L. (1995). - Discontinuities in carbonate successions: identification, interpretation and classification of some Italian examples. - *Sedimentary Geology*, **100**, 97–121.
- CRUMEYROLLE, P., LESUEUR, J.L., CLAUDE, D., et JOSEPH, P. (1992). - Architecture et faciès d'un prisme deltaïque de bas niveau marin : les Grès de Roda (Bassin Éocène Sud Pyrénéen). Livret-guide de l'excursion ASF (Association des Sédimentologues Français) du 25-27 Septembre 1992, Publication ASF n° 17, 76 p, <http://www.sedimentologie.com/>
- CUEVAS-GOZALO M., DONSELAAR M.E. & NIO S.D. (1985). - Eocene clastic tidal deposits in the Tremp-Graus Basin (Provs. of Lerida and Huesca). - 6th European Regional Meeting IAS, Lerida, Guidebook Excursion n°6, 215-266.

- DICKSON J.A.D. (1966). - Carbonate identification and genesis as revealed by staining. - *Journal of Sedimentary Research*, **36**, 2, 491-505.
- DICKSON J.A.D. & SALLER A.H. (1995). – Identification of subaerial exposure surfaces and porosity preservation in Pennsylvanian and Lower Permian shelf limestones, eastern Central basin platform, Texas. In : D.A. BUDD, A.H. SALLER and P.M. HARRIS, Eds, Unconformities and porosity in carbonate strata. – AAPG Mem., **63**, 239-258.
- DURLET C. & LOREAU J.P. (1996). - Séquence diagénétique intrinsèque des surfaces durcies: mise en évidence de surface d'émersion et de leur ablation marine. Exemple de la plate-forme bourguignonne, Bajocien (France). – *C. R. Acad. Sci., Paris*, **323**, 389-396.
- 10 EICHENSEER H. (1988). - Facies Geology of Late Maestrichtian to Early Eocene coastal and shallow marine sediments (Trempe-Graus Basin, Northeastern Spain). - Ph.D. Thesis, Univ. Tübingen, Germany, 237 p.
- EICHENSEER H. & LUTERBACHER H. (1992). - The Marine Paleogene of the Trempe Region (NE Spain) - Depositional Sequences, Facies History, Biostratigraphy and Controlling Factors. - *Facies*,
15 **27**, 119-152.
- EMBRY, A.F. (1993). - Transgressive-regressive (T-R) sequence analysis of the Jurassic succession of the Sverdrup Basin, Canadian Arctic Archipelago. *Canadian Journal of Earth Sciences*, 30, 301-320.
- EMERY D. & MYERS K.J. (1996). - Sequence Stratigraphy. - Blackwell Science Ltd, 297 p.
- FONNESU F. (1984). - Estratigrafia física y análisis de facies de la secuencia de Figols entre el Rio Noguera Pallaresa e Iscles (Prov. de Lerida y Huesca). - Ph.D. Thesis, Fac. Ciencias Univ. Auton. Barcelona, Spain, 317 p.
- 20 FRIEDRICH O., SCHMIEDL G., ERLLENKEUSER H. (2006). - Stable isotope composition of Late Cretaceous benthic foraminifera from the southern South Atlantic: Biological and environmental effects. - *Marine Micropaleontology*, **58**, 135– 157.

- GARRIDO-MEGIAS A. & RIOS L.M. (1972). - Sintesis geologica del Secundario y Terciario entre los rios Cinca y Segre (Pirineo Central de la vertiente surpirenaica, provincias de Huesca y Lerida). - *Bol. Geol. Min.*, **LXXXIII**, 1-47.
- 5 GASSE F., FONTES J.C., PLAZIAT J.C., CARBONEL P., KACZMARSKA I., DE DECKKER P., SOULIE-MARSCHE I., CALLOT I. & DUPEUBLE P.A. (1987). - Biological remains, geochemistry and stable isotopes for the reconstruction of environmental and hydrological changes in the Holocene lakes from North Sahara. - *Palaeogeogr. Palaeoclimatol. Palaeoecol.*, **60**, 1 – 46.
- GEEL T. (2000). - Recognition of stratigraphic sequences in carbonate platform and slope deposits: empirical models based on microfacies analysis of Paleogene deposits in Southeastern Spain. -
 10 *Palaeogeography, Palaeoclimatology, Palaeoecology*, **155**, 211-238.
- GRADSTEIN F.M., OGG J.G. & SMITH A.G. (2004). - A geologic time scale. - Cambridge University Press, Cambridge, UK, 610 p.
- GRAF D. L. (1960). Geochemistry of carbonate sediments and sedimentary carbonate rocks. Part I : Carbonate Mineralogy, Carbonate Sediments. - *Illinois State Geological Survey*, 39 p.
- 15 HAMON Y., SANTERRE Y., GRANJEON D., CONESA G. & BORGOMANO J. (2013). - Early diagenesis in meteoric versus brackish environments: Example of the Late Oligocene-Early Miocene, littoral, mixed sedimentary succession of Carry-Le-Rouet (southeastern France). - *Bull. Soc. géol. France*, **184**, 6, 601-620.
- HARDIE L.A. (1996). - Secular variation in seawater chemistry: An explanation for the coupled
 20 secular variation in the mineralogies of marine limestones and potash evaporites over the past 600 m.y. – *Geology*, **24**, 279-283.
- HAY W.W., DECONTO R., WOLD C.N., WILSON K.M., VOIGT S., SCHULZ M., WOLD-ROSSBY A., DULLO W.C., RONOVA A.B., BALUKHOVSKY A.N. & SOEDING E. (1999). - Alternative Global Cretaceous Paleogeography. *In*: E. BARRERA and C. JOHNSON, Eds, The
 25 Evolution of Cretaceous Ocean /Climate Systems. - GSAB Spec. Paper, 332, Boulder, Colorado, 1-47.

- HILLGARTNER H. (1998). - Discontinuity surfaces on a shallow-marine carbonate platform. - *Journal of Sedimentary Research*, **68**, 1093-1108.
- HOTTINGER L. (1960). - Recherches sur les Alvéolines du Paléocène et de l'Eocène. - *Mem. Suisses Paleont.*, **75-76**, 243 p.
- 5 HOTTINGER L. (1997). - Shallow benthic foraminiferal assemblages as signals for depth of their deposition and their limitations. - *Bulletin de la Société Géologique de France*, **168**, 491-505.
- IMMENHAUSER A., SCHLAGER W., BURNS S.J., SCOTT R.W., GEEL T., LEHMANN J., VAN DER GAAST S. & BOLDER-SCHRIJVER L.J.A. (2000). - Origin and correlation of disconformity surfaces and marker beds, Nahr Umr Formation, Northern Oman. *In*: A.S. ALSHARHAN and R.W. SCOTT, Eds., Middle East Models of Jurassic/Cretaceous Carbonate Systems. - *SEPM Special Publication*, **69**, 209–225.
- 10
- JOACHIMSKI M.M. (1994). - Subaerial exposure and deposition of shallowing upward sequences: evidence from stable isotopes of Purbeckian peritidal carbonates (basal Cretaceous), Swiss and French Jura Mountains. - *Sedimentology*, **41**, 805-824.
- 15
- KABANOV P., ANADÓN P. & KRUMBEIN W.E. (2008). - *Microcodium*: An extensive review and a proposed non-rhizogenic biologically induced origin for its formation. - *Sedimentary Geology*, **205**, 79–99.
- KAUFMAN L. & ROUSSEEUW P.J. (1990). - Finding Groups in Data: An Introduction to Cluster Analysis. - Wiley Series in Probability and Statistics, Wiley, New York, 368 p.
- 20
- KOSIR A. (2004). - *Microcodium* revisited: root calcification products of terrestrial plants on carbonate-rich substrates. – *Journal of Sedimentary Research*, **74**, 6, 845–857.
- KRUMBEIN W.E. & JENS K. (1981). - Biogenic rock varnishes of the Negev Desert (Israel): an ecological study of Iron and Manganese transformation by cyanobacteria and fungi. - *Oecologia*, **50**, 25-38.

- LENTZ D. R. (2003). - Geochemistry of Sediments and Sedimentary Rocks: Evolutionary Considerations to Mineral Deposit-Forming Environments. - *Geological Association of Canada*, 184p.
- LETURCQ T. (1999). - Dynamique récifale à l'Ilerdien : exemple du bassin de Graus-Tremp (Pyrénées, Espagne). - Ph.D. Thesis, Université Paris VI, France, 376 p.
- 5 LOHMANN K. C. (1988). - Geochemical patterns of meteoric diagenetic systems and their application to studies of paleokarst. *In: JAMES N.P. & CHOQUETTE P.W., Eds., Paleokarst.* - Springer-Verlag New-York, 58-80.
- LOPEZ-BLANCO M., MARZO M. & MUÑOZ J.A. (2003). - Low-amplitude, synsedimentary folding of a deltaic complex: Roda Sandstone (lower Eocene), South-Pyrenean Foreland Basin. -
10 *Basin Research*, **15**, 73-95.
- LUKASIK J. & JAMES N.P. (2003). - Deepening-upward subtidal cycles, Murray Basin, South Australia. - *Journal of Sedimentary Research*, **73**, 653-671.
- LUTERBACHER H.P., EICHENSEER H., BETZLER CH. & VAN DEN HURK A.M. (1991). -
Carbonate-siliciclastic depositional systems in the Paleogene of the South Pyrenean foreland basin: a
15 sequence-stratigraphic approach. - *Spec. Publ. Int. Ass. Sediment.*, **12**, 391-407.
- MADHAVARAJU J. (2015). Geochemistry of late cretaceous sedimentary rocks of the Cauvery Basin, South India: Constraints on paleoweathering, provenance, and end Cretaceous environments. *In: M. RAMKUMAR, Ed., Chemostratigraphy: Concepts, Techniques, and Applications.* - Elsevier Publisher, 185-214.
- 20 MARQUES W.S., SIAL A.N., DE ALBUQUERQUE MENOR E., FERREIRA V.P., SA´ FREIRE G.S., DE ALBUQUERQUE MEDEIROS LIMA E. & DO AMARAL VAZ MANSO V. (2008). - Principal component analysis (PCA) and mineral associations of litoraneous facies of continental shelf carbonates from northeastern Brazil. - *Continental Shelf Research*, **28**, 2709–2717.

- MATEU-VICENS G., POMAR L. & FERRANDEZ-CANADELL C. (2012). - Nummulitic banks in the upper Lutetian 'Buil level', Ainsa Basin, South Central Pyrenean Zone: the impact of internal waves. – *Sedimentology*, **59**, 527–552.
- MEY P.W.H., NAGTEGAAL P.J.C., ROBERTI K.J. & HARTEVELT J.J.A. (1968). -
5 Lithostratigraphic subdivision of posthercynian deposits in the South-Central Pyrenees, Spain. - *Leidse Geol. Meded.*, **41**, 221-228.
- MIDDLETON G.V. (1991). - A short historical review of clastic tidal sedimentology. *In*: D.G. SMITH, G.E. REINSON, B.A. ZAITLIN and R.A. RAHMANI, Eds, *Clastic Tidal Sedimentology*. - Canadian Society of Petroleum Geology Memoir, **16**, Calgary, Canada, ix-xv.
- 10 MOLINA E., ANGORI E., ARENILLAS I., BRINKHUIS H., CROUCH E.M., LUTERBACHER H., MONECHI S. & SCHMITZ B. (2003). - Correlation between the Paleocene/Eocene boundary and the Ilerdian at Campo, Spain. - *Revue de micropaleontology*, **46**, 95-109.
- MOORE C.H. (2001). - Carbonate Reservoirs. Porosity Evolution and Diagenesis in a sequence Stratigraphic Framework. - *Developments in Sedimentology*, **55**, Elsevier Science Ltd., Amsterdam
15 (Nederland), 460 p.
- MORSE J. W. (2003). Formation and Diagenesis of Carbonate Sediments. *In*: F. T. MACKENZIE, Ed., *Sediments, Diagenesis, and Sedimentary Rocks. Treatise on Geochemistry, Volume 7*. – Elsevier Publisher, 67-85.
- MORSILLI M., BOSELLINI F.R., POMAR L., HALLOCK P., AURELL M. & PAPAZZONI C.A.
20 (2012). - Mesophotic coral buildups in a prodelta setting (Late Eocene, southern Pyrenees, Spain): a mixed carbonate–siliciclastic system. - *Sedimentology*, **59**, 766–794.
- MUNOZ J.A. (1992). - Evolution of a continental collision belt: ECORS-Pyrenees crustal balanced cross-section. *In*: K. R. McCLAY, Ed., *Thrust Tectonics*. Springer Netherlands, 235–246.

- MUTTI E., SEGURET M. & SGAVETTI M. (1988). - Sedimentation and Deformation in the Tertiary Sequences of the Southern Pyrenees. - Guide Book of Field Trip 7, AAPG Mediterranean Basins Conference, Nice, France, Special Publication of the Institute of Geology of the University of Parma, 157 p.
- 5 NIJMAN W. & NIO S.D. (1975). - The Eocene Montañana delta. *In*: J. ROSELL and C. PUIGDEFABREGAS, Eds, Sedimentary evolution of the Paleogene South Pyrenean Basin. - 9th International Congress I.A.S., Nice, part B, 56 p.
- OLARIU C., STEEL J., DALRYMPLE R.W. & GINGRAS K. (2012). - Tidal dunes versus tidal bars: The sedimentological and architectural characteristics of compound dunes in a tidal seaway, the lower
10 Baronia Sandstone (Lower Eocene), Ager Basin, Spain. - *Sedimentary Geology*, **279**, 134-155.
- ORI G. & FRIEND P. (1984). - Sedimentary basins formed and carried piggyback on active thrust sheets. - *Geology*, **12**, 475-478.
- PAYROS A., PUJALTE V., BACETA J.I., BERNAOLA G., ORUE-ETXEBARRIA X., APPELANIZ E., CABALLERO F. & FERRANDEZ C. (2000). - Lithostratigraphy and sequence
15 stratigraphy of the Upper Thanetian to Middle Ilerdian Strata of the Campo Section (Southern Pyrenees, Spain): Revision and new data. - *Rev. Soc. Geol. España*, **13**, 2, 213-226.
- PERRIN C. (1992). - Signification écologique des Foraminifères Acervulinidés et leur rôle dans la formation de faciès récifaux et organogènes depuis le Paléocène. - *Geobios*, **25**, 725-751.
- PLAZIAT J.C. (1975). - L'Ilerdien à l'intérieur du Paléogène languedocien; ses relations avec le
20 Sparnacien, l'Ilerdien sud-Pyrénéen, l'Yprésien et le Paléocène. - *Bulletin de la Société géologique de France*, **XVII**, 168-181.
- PLAZIAT J.C. (1984). - Le domaine pyrénéen de la fin du Crétacé à la fin de l'Eocène. Stratigraphie, paléo-environnements et évolution paléogéographique. Ph.D. Thesis, Université Paris-Sud, France, 1362 p.

- PLAZIAT J.C. & PERRIN C. (1991). - Multikilometer-sized reefs built by Foraminifera (Solenomeris) from the early Eocene of the Pyrenean domain (S. France, N. Spain) : Palaeoecologic relations with coral reefs. - *Palaeogeography, Palaeoclimatology, Palaeoecology*, **96**, 195-223.
- POMAR L. (2001). - Types of carbonate platforms: a genetic approach. - *Basin Research*, **13**, 313-334.
- POMAR L., MATEU-VICENS G., MORSILLI M. & BRANDANO M. (2014). - Carbonate ramp evolution during the Late Oligocene (Chattian), Salento Peninsula, southern Italy. - *Palaeogeography, Palaeoclimatology, Palaeoecology*, **404**, 109–132.
- POMONI-PAPAIOANNOU F.A. & KOSTOPOULOU V. (2010). - Subaerial exposure-related discontinuities in shallow-water platform carbonate successions (Late Triassic-Pelagonian & Early Jurassic-Gavrovo Tripolitza, Greece). - *Hellenic Journal of Geosciences*, **45**, 227-238.
- PUJALTE V., BACETA J.I., SCHMITZ B., ORUE-ETXEBARRIA X., PAYROS A., BERNAOLA G., APELLANIZ E., CABALLERO F., ROBADOR A., SERRA-KIEL J. & TOSQUELLA J. (2009). - Redefinition of the Ilerdian Stage (early Eocene). - *Geologica Acta*, **7**, 1-2, 177-194.
- PURSER B.H. (1980). - Sédimentation et diagenèse des carbonates néritiques récents (Tome 1). - Société des Editions Technip, Paris, France, 388 p.
- QUINN T.M. (1991). – Meteoric diagenesis of Plio-Pleistocene limestones at Enewetak Atoll. – *J. Sediment. Res.*, **61**, 5, 681-703.
- RASSER M.W., SCHEIBNER C. & MUTTI M. (2005). - A paleoenvironmental standard section for Early Ilerdian tropical carbonate factories (Corbières, France; Pyrenees, Spain). - *Facies*, **51**, 217-232.
- READ J.F. (1998). - Phanerozoic carbonate ramps from greenhouse, transitional and ice-house worlds: clues from field and modelling studies. - *Geological Society of London Special Publications*, **149**, 107-135.

- READING H.G. (1996). - Sedimentary Environments: Process, Facies and Stratigraphy – Third Edition. - Blackwell Science, 688 p.
- REMACHA E. & ZAMORANO M. (1989). - Reflejo de la estratigrafía secuencial del Eoceno inferior surpirenaico en una parte de la sección de Campo. – *Geogaceta*, **6**, 94-96.
- 5 REY J. & BOUSQUET J.-P. (1981). - Observations préliminaires sur les paléoenvironnements de l'Ilerdien de Coustouge (Corbières, France). - *Geobios*, **14**, 5, 655-659.
- RODUIT N. (2008). - JMicroVision: image analysis toolbox for measuring and quantifying components of high-definition images. - <http://www.jmicrovision.com/index.htm>.
- ROURE F., CHOUCROUNE P., BERASTEGUI X., MUNOZ J.A., VILLIEN A., MATHERON P.,
10 BAREYT M., SÉGURET M., CAMARA P. & DERAMOND J. (1989). - Ecoregional deep seismic data and balanced cross-section: geometric constraints on the evolution of the Pyrenees. - *Tectonics*, **8**, 41-50.
- SAGEMAN B. B. & LYONS T. W. (2003). - Geochemistry of Fine-grained Sediments and Sedimentary Rocks. *In*: F. T. MACKENZIE, Ed., Sediments, Diagenesis, and Sedimentary Rocks. Treatise on Geochemistry, Volume 7. – Elsevier Publisher, 115-158.
- 15 SATTLER U., IMMENHAUSER A., HILLGÄRTNER H. & ESTEBAN M. (2005). - Characterization, lateral variability and lateral extent of discontinuity surfaces on a carbonate platform (Barremian to Lower Aptian, Oman). - *Sedimentology*, **52**, 339–361.
- SCHEIBNER C., RASSER M.W. & MUTTI M. (2007). - The Campo Section (Pyrenees, Spain) revisited: Implications for changing benthic carbonate assemblages across the Paleocene-Eocene
20 boundary. - *Palaeogeography, Palaeoclimatology, Palaeoecology*, **248**, 145-168.
- SCHEIBNER C. & SPEIJER R.P. (2008). - Late Paleocene–early Eocene Tethyan carbonate platform evolution - A response to long- and short-term paleoclimatic change. - *Earth-Science Reviews*, **90**, 71-102.

- SCHLAGER W. (2005). - Carbonate Sedimentology and Sequence Stratigraphy. - *SEPM Concepts in Sedimentology and Paleontology Series*, **8**, 200 p.
- SCHMIEDL G., PFEILSTICKER M., HEMLEBEN C., MACKENSEN A. (2004). - Environmental and biological effects on the stable isotope composition of recent deep-sea benthic foraminifera from the western Mediterranean Sea. - *Marine Micropaleontology*, **51**, 129– 152.
- SCHMITZ B., ASARO F., MOLINA E., MONECHI S., VON SALIS K. & SPEIJER R.P. (1997). - High-resolution iridium, $\delta^{13}\text{C}$, $\delta^{18}\text{O}$, foraminifera and nannofossil profiles across the latest Paleocene benthic extinction event at Zumaya, Spain. - *Palaeogeography, Palaeoclimatology, Palaeoecology*, **133**, 49–68.
- 10 SCHMITZ B. & PUJALTE V. (2003). - Sea-level, humidity, and land-erosion records across the initial Eocene thermal maximum from a continental–marine transect in northern Spain. - *Geology*, **31**, 689–692.
- SCHMITZ B. & PUJALTE V. (2007). - Abrupt increase in seasonal extreme precipitation at the Paleocene–Eocene boundary. – *Geology*, **35**, 215–218.
- 15 SCHOLLE P.A., BEBOUT D.G. & MOORE C.H. (1983). - Carbonate depositional environments. - *AAPG Memoir 33*, AAPG, Tulsa, Oklahoma, 708 p.
- SEGURET M. (1972). - Étude tectonique des nappes et séries décollées de la partie centrale du versant sud des Pyrénées – caractère synsédimentaire, rôle de la compression et de la gravité. - *Série géologie structurale 2*, Publications de l'Université des Sciences et
- 20 Techniques du Languedoc (USTELA), Montpellier, France, 155 p.
- SERRA-KIEL J., CANUDO J.I., DINARES J., MOLINA E., ORTIZ N., PASCUAL J.O., SAMSO J.M. & TOSQUELLA J. (1994). - Chronostratigraphía de los sedimentos marinos del Terciario inferior de la Cuenca de Graus-Tremp (Zona Central Surpirenaica). - *Rev. Soc. Geol. España*, **7**, 3-4, 273-297.

- SHERMAN C.E., FLETCHER C.H. & RUBIN K.H. (1999). Marine and meteoric diagenesis of Pleistocene carbonates from a nearshore submarine terrace, Oahu, Hawaii. – *Journal of Sedimentary Research*, **69** (5), 1083-1097.
- 5 SLOAN L.C. & THOMAS E. (1998). - Global climate of the late Paleocene epoch: modeling the circumstances associated with a climatic “event”. *In*: M.P. AUBRY, S. LUCAS, W.A. BERGGREN, Eds, Late Paleocene–early Eocene climatic and biotic events in the marine and terrestrial records. - Columbia University Press, New York, 138–157.
- 10 STRASSER A. & HILLGÄRTNER H. (1998). - High-frequency sea-level fluctuations recorded on a shallow carbonate platform (Berriasian and Lower Valanginian of Mount Salève, French Jura). - *Ecolgae Geologicae Helvetiae*, **91**, 375-390.
- TOSQUELLA J. (1988). - Estudi sedimentològic i biostratigràfic de la Formació Gresos de Roda (Eocè, Conca de Tremp-Graus). - Tesis Licenciatura, Univ. Barcelona, Spain, 540 p.
- TUCKER M.E. & WRIGHT V.P. (1992). - Carbonate Sedimentology. - Blackwell scientific publications, Oxford, UK, 482 p.
- 15 VEIZER J., ALA D., AZMY K., BRUCKSCHEN P., BUHL D., BRUHN F., CARDEN G.A.F., DIENER A., EBNETH S., GODDERIS Y., JASPER T., KORTE C., PAWELLEK F., PODLAHA O.G. & STRAUSS H. (1999). $^{87}\text{Sr}/^{86}\text{Sr}$, $\delta^{13}\text{C}$ and $\delta^{18}\text{O}$ evolution of Phanerozoic seawater. *Chemical Geology*, **161**, 59-88.
- 20 VINCENT S.J. (2001). - The Sis palaeovalley: a record of proximal fluvial sedimentation and drainage basin development in response to Pyrenean mountain building. - *Sedimentology*, **48**, 1235-1276.
- WACHTER E. & HAYES J.M. (1985). - Exchange of oxygen isotopes in carbon-dioxide-phosphoric acid systems. - *Chemical Geology*, **52**, 365-374.

- WALKER R.G. (1992). - Facies, facies models and modern stratigraphic concepts. *In*: R.G. Walker, and N.P. James, Eds, Facies Models, Response to Sea Level Change. - Geological Association of Canada, St. John's, Newfoundland, 1-14.
- 5 WEBB G.E., NOTHDURFT L.D., KAMBER B.S., KLOPROGGE J.T. & ZHAO J.-X. (2009). - Rare earth element geochemistry of scleractinian coral skeleton during meteoric diagenesis: a sequence through neomorphism of aragonite to calcite. – *Sedimentology*, **56(5)**, 1433–1463.
- WILSON J.L. (1975). - Carbonate facies in Geologic History. - Springer-Verlag, Berlin-Heidelberg-New York, 471 p.
- 10 WOLD S., ESBENSEN K. & GELADI P. (1987). - Principal component analysis. - *Chemom. Intell. Lab. Syst.*, 2, 37-52.
- WOOD R. (1999). - Reef evolution. - Oxford University Press, Oxford, 426 p.
- WOODY D.T., SMITH J.J., KRAUS M.J. & HASIOTIS S.T. (2014). – Manganese-bearing rhizoconcretions in the Willwood Formation, Wyoming, USA: Implications for paleoclimate during the Paleocene-Eocene thermal maximum. – *Palaios*, **29(6)**, 266-276.
- 15 ZACHOS J., PAGANI M., SLOAN L., THOMAS E. & BILLUPS K. (2001). Trends, rhythms, and aberrations in global climate 65 Ma to present. - *Science*, **292**, 686–693.

Figure captions

- Figure 1:** A) Geological map of the south-central Pyrenees (modified from Vincent [2001]) and location of the study area (Serraduy). B) Geological map showing the main lithostratigraphic formations of Early Eocene age in the Rigaborzana area (modified from Mapa Geologic de Catalunya 1:250000). C) Geological map showing the main lithostratigraphic formations of Early Eocene age in the Serraduy area, with location of the
- 20

sedimentary sections described in this study and correlation plate of Fig. 5 in red (UTM coordinates, WGS84) (modified from Mapa Geologic de Catalunya 1:250000).

Figure 2: General stratigraphy (names of formations are informal), main lithologies and depositional environments of the Early Eocene series of the Graus-Tremp Basin. Paleogene zonation of larger foraminifera (Gradstein *et al.*, 2004 and Serra-Kiel *et al.*, 1994).

Figure 3: A) Field photograph showing facies A1, heterometric and heterolithic conglomerate. B) Field photograph showing facies B2, interstratified with B1. C) Field photography showing prograding sets of the B1 facies forming a lobe structure. D) General view of the main cliff studied in the Serraduy area (geobodies and bounding surfaces are underlined). E) General view of the deltaic complex in the Serraduy area (underlined bodies). The deltaic lobes show compensations cycles and are largely incised at their top by a deeply-scoured channel filled by a tidal megadune (facies C4). F) Field photography showing one of the build-ups that developed over the surface S3 (central part of the outcrops) and corresponding line drawing and facies interpretation. G) Field photography showing another build-up (South Serraduy) that developed over the surface S3, overlain by facies D1, E1 and E2. H) Field photography showing the geometry of the build-up observed in the Northern part of the Serraduy area, developed during the first small-scale cycle.

Figure 4: A) Transmitted light plane-polarized (PPL) photomicrograph showing facies B1 (dominated by quartz and *Microcodium* fragments) and small Miliolids (white arrow). B) PPL photomicrograph showing facies B1, dominated by quartz and *Microcodium* fragments (white arrow). C) PPL photomicrograph showing facies B3, a bioclastic sandy limestone. Presence of green algae (black arrows), serpulids, gastropods, Miliolids (white arrow). D) PPL photomicrograph showing facies B4, dominated by gastropods (black arrows) and Orbitolite fragments (white arrows) in a silty mudstone matrix. E) Transmitted light crossed-polarized (XPL) photomicrograph of facies C1 composed of a wackestone-packstone dominated by

Alveolina (white arrows), *Orbitolites* (black arrows) and Miliolids (grey arrows). F) PPL photomicrograph of C3 (micro-grainstone dominated by Miliolids, intraclasts and echinoids debris). G) PPL photomicrographs showing the facies C4, that fills the incision in Serraduy (micrograinstone with intraclasts and miliolids). H) PPL photomicrograph showing facies D1 (*Alveolina* (white arrows)–*Nummulites* (black arrows) wackestone). I) PPL photomicrograph showing *Operculina*-dominated wackestone (facies D2). In this example, *Operculina* (white arrows) are associated to pelecypod and echinoid debris. J) PPL photomicrograph showing facies E1 (*Assilina* (black arrows)-dominated wackestone, *Operculina* (white arrows)). K) PPL photomicrograph showing facies F2 composed of coral (black arrow) encrusted by red algae (white arrow). L) PPL photomicrograph showing facies F3 dominated by the red algae-*Solenomeris* association (white arrows).

Figure 5: 3D-Model illustrating the general architecture of the Ilerdian *Alveolina Limestone* Fm. in the Serraduy area (location on Fig. 1). Facies and boundaries of the small-scale cycles (bold lines, named as S0 to S5) and associated architectures are highlighted. The location of the different field photographs of Fig. 3 are specified.

Figure 6: A) Conceptual depositional model for the Ilerdian *Alveolina Limestone* Fm. in the Serraduy area, and distribution of the main sedimentary facies. B) Sequence stratigraphy framework of the series, showing the identification of five small-scale cycles.

Figure 7: Cross-plot of $\delta^{13}\text{C}_{\text{V-PDB}}$ versus $\delta^{18}\text{O}_{\text{V-PDB}}$ values for three sections: AB (diamond), H (triangles) and N (circles). Samples with white symbols correspond to *Alveolina*, gray symbols correspond to *Nummulites*, and black symbols correspond to bulk, dominated by *Microcodium* debris.

Figure 8: Results of $\delta^{13}\text{C}_{\text{V-PDB}}$ and $\delta^{18}\text{O}_{\text{V-PDB}}$ analysis, plotted vertically along the three studied sections AB, H and N. The different cycles and their bounding discontinuities (S0 to

S5) are also mentioned. Samples with white circles correspond to *Alveolina*, gray circles correspond to *Nummulites*, and black circles correspond to bulk, dominated by *Microcodium* debris.

Figure 9: A) PCA projection of the variables studied (without SiO) on the principal axes 1 and 2 (left) and axes 1 and 3 (right). Principal components 1 and 2 represent 70.52% of the total variability (53.36% and 17.15% respectively) whereas the projections on axes 1 and 3 represent 64.31% of the total variability (53.36% and 10.94% respectively). B) Biplots corresponding to a representation of the analysed samples in the PCA space presented in Fig. 9A. Siliciclastic-dominated, carbonate-dominated samples are respectively highlighted in green and blue. Samples located below discontinuities S1 and S3 are shown in red. Scattered values outside of these domains correspond to lag deposits. C) PCA projection of the variables studied (elemental geochemistry subset including SiO analysis) on the principal axes 1 and 2 (left) and axes 1 and 3 (right). Principal components 1 and 2 represent 76.17% of the total variability (64.66% and 11.51% respectively) whereas the projections on axes 1 and 3 represent 75.40% of the total variability (64.66% and 10.74% respectively).

Figure 10: Results of major (Mg in %), minor (Al, Fe, K in %) and trace elements (Mn, Ti, Sr, Na in ppm), plotted vertically along the two studied sections AB and N. The different sedimentary discontinuities (S0 to S5) are also mentioned.

Figure 11: Dendrogram resulting from the AHC performed on the carbonate-dominated samples of the dataset. All the observations are grouped into three main categories. The dotted line represents the automatic truncation. Sample C11 is an atypical value.

Figure 12: Sequence stratigraphy for the Serraduy area with proximal to distal evolution of the systems tracts.

Table 1: Isotopic and elemental geochemistry analyses realized on the three studied sections AB, N and H.

Table 2: A) PCA correlation matrix showing correlation coefficient calculated with the elemental geochemistry dataset (without SiO). B) PCA correlation matrix showing correlation coefficient calculated with the elemental geochemistry subset including SiO analysis.

5

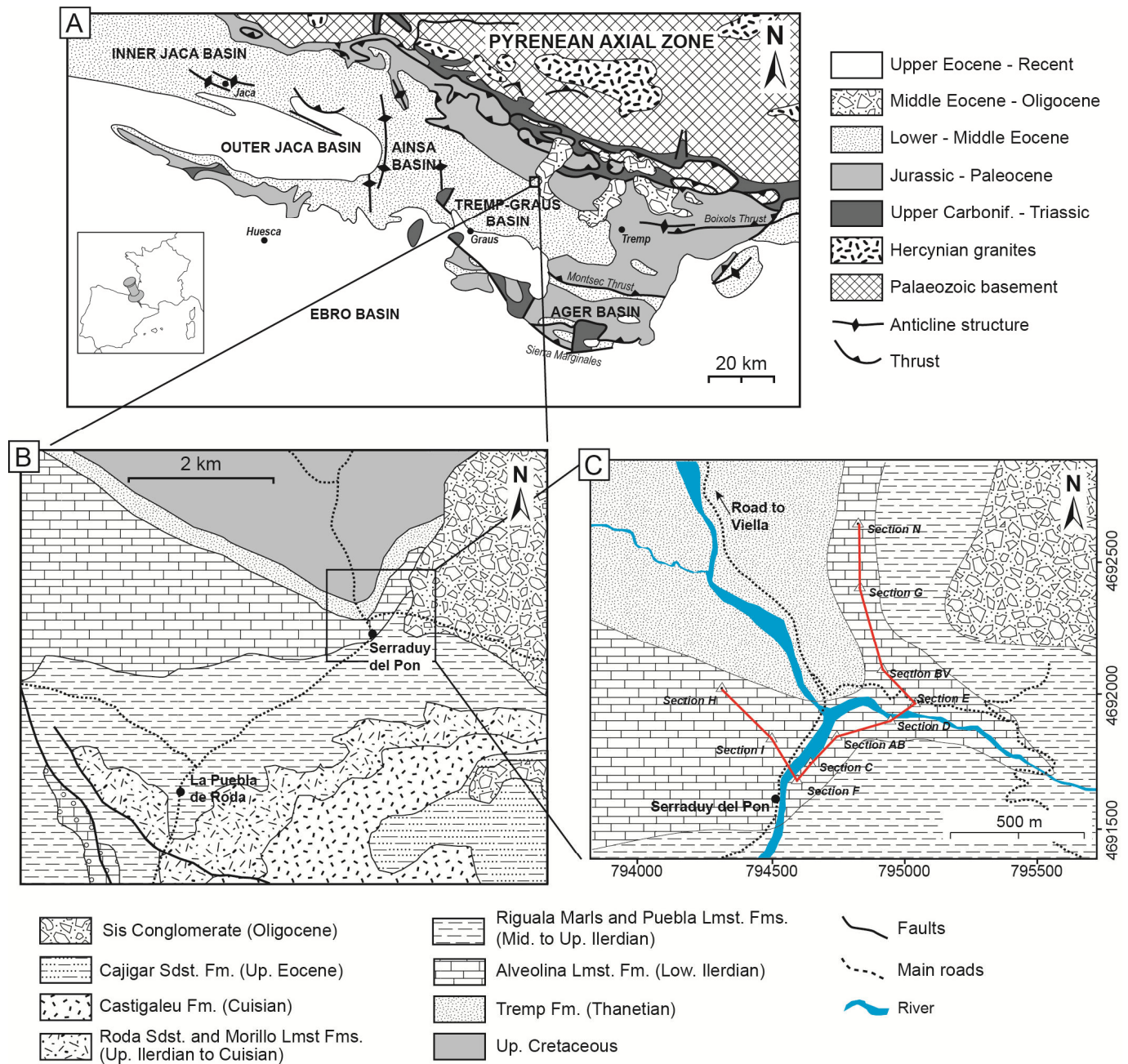


Figure 1

Age	Formation	Litho.	Depo. env.	Paleogene zonations of larger foram.			
				Serra-Kiel <i>et al.</i> , 1994	Gradstein <i>et al.</i> , 2004		
Early Eocene (Ypresian)	Cuisian	Morillo Lmst.	Inner ramp				
		Roda Sandstone	Deltaic system	<i>Alveolina oblonga</i>	<i>Nummulites planulatus</i>	SBZ10	
	Ilerdian	Puebla Lmst.	Mid ramp		<i>A. trempina</i>	<i>N. involutus</i>	SBZ9
		Riguala Marls	Mid to outer ramp		<i>Alveolina corbarica</i>	<i>Nummulites exilis</i>	SBZ8
		Alveolina Limestone	Inner to mid ramp Deltaic system		<i>Alveolina moussoulensis</i>	<i>Nummulites robustiformis</i>	SBZ7
					<i>Alveolina ellipsoidalis</i>	<i>Nummulites fraasi</i>	SBZ6
					<i>Alveolina cucumiformis</i>		SBZ5
Palaeoc. Thanetian	Tresp	Coastal plain Braided system		<i>Glomalv. levis</i>	<i>Assilina yvettae</i>	SBZ4	
				<i>Glomalv. primaeva</i>		SBZ3	

Figure 2

5

10

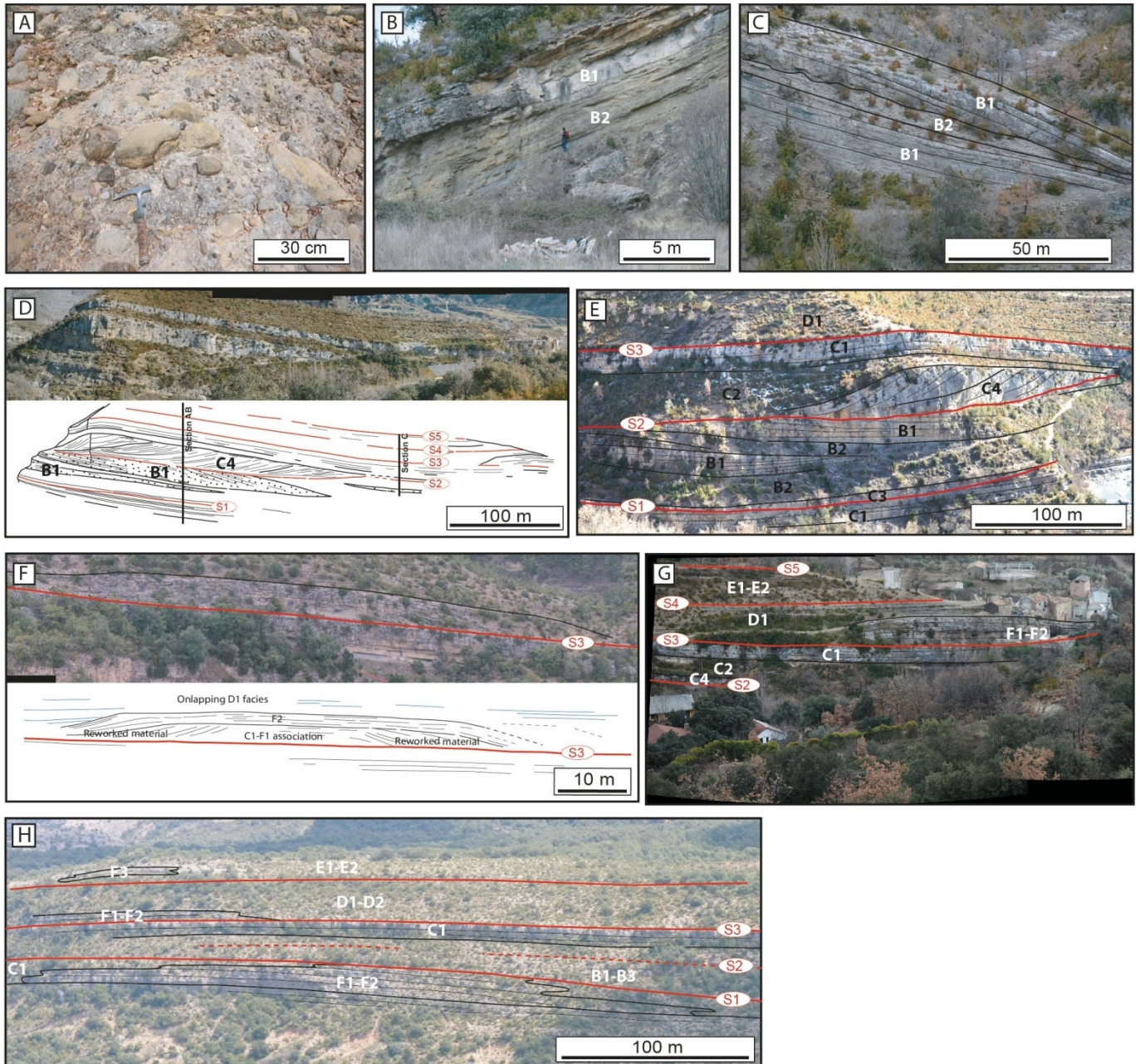


Figure 3

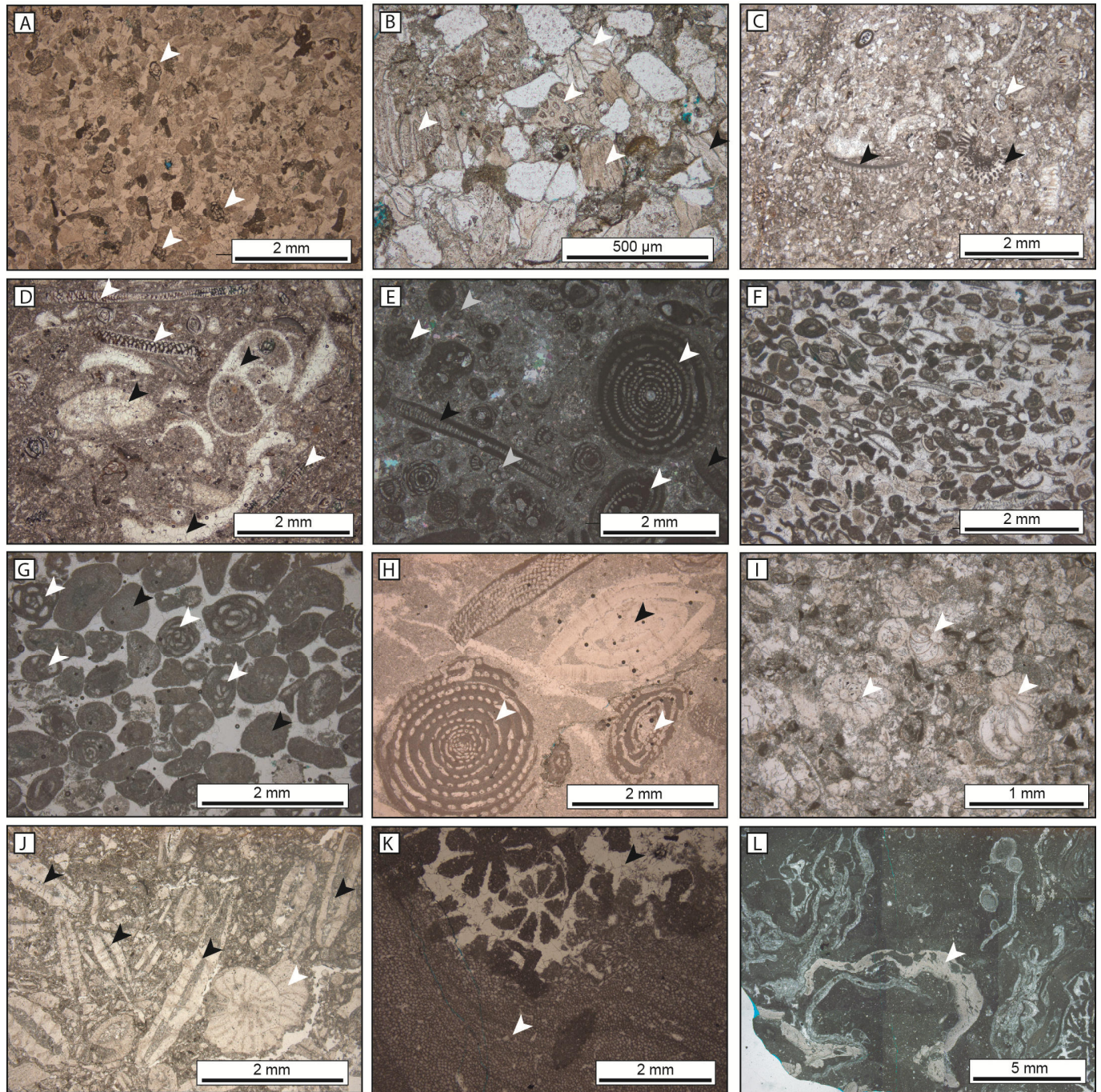


Figure 4

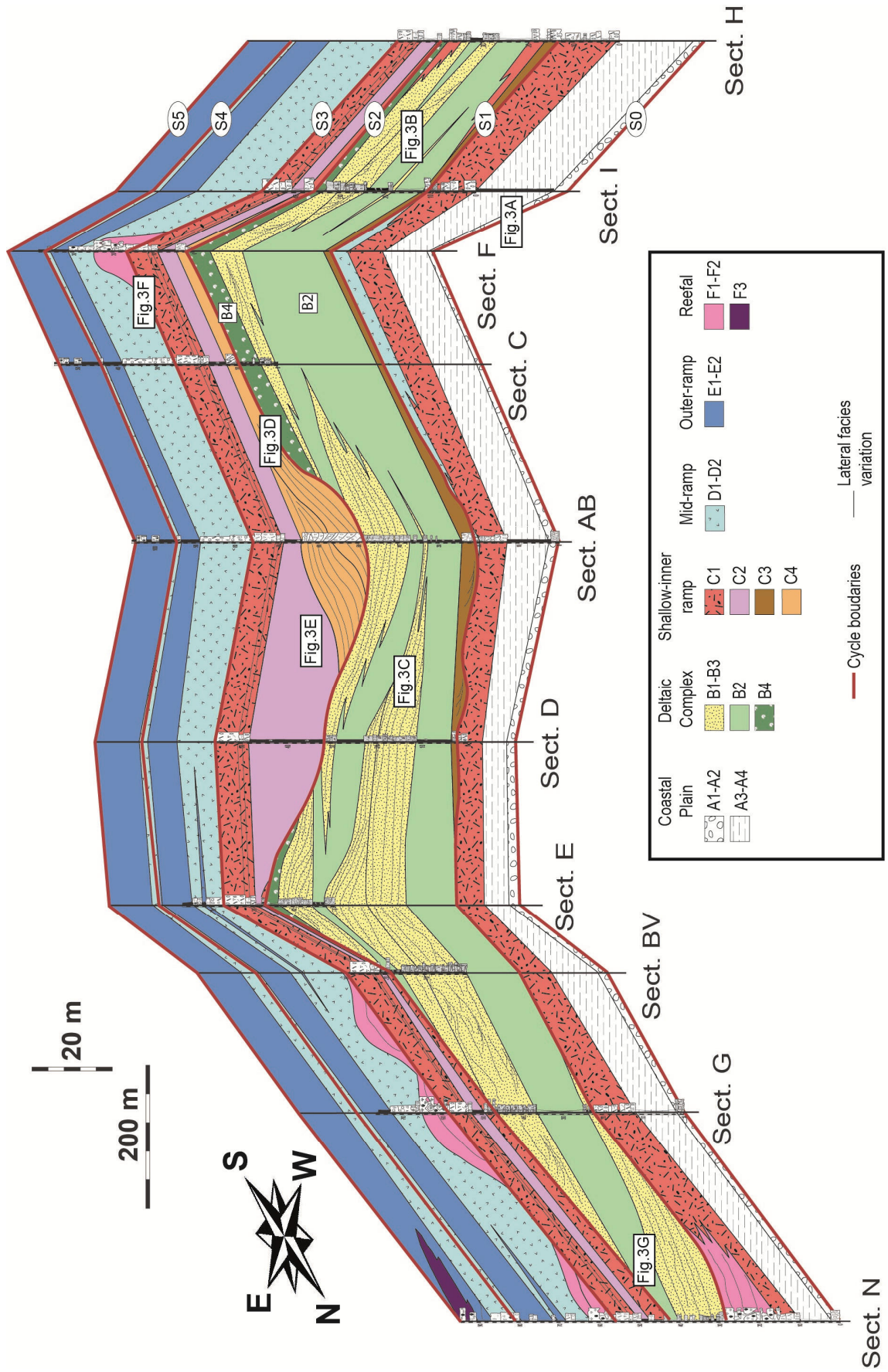


Figure 5

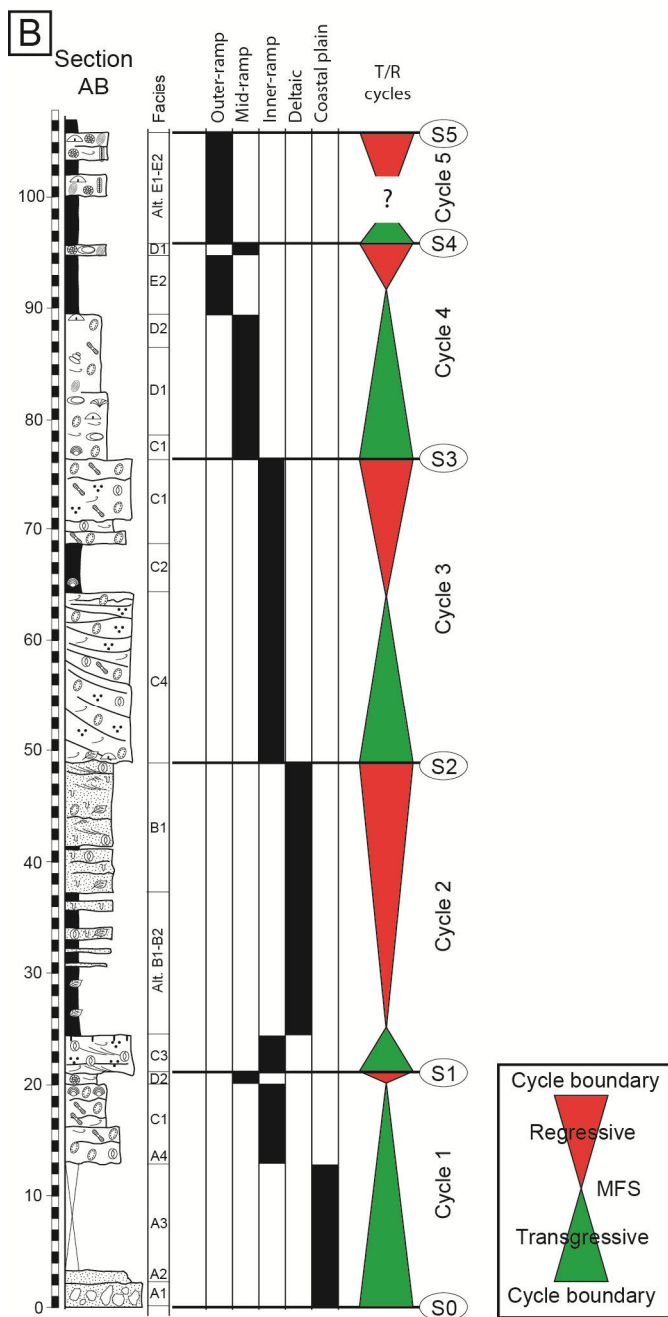
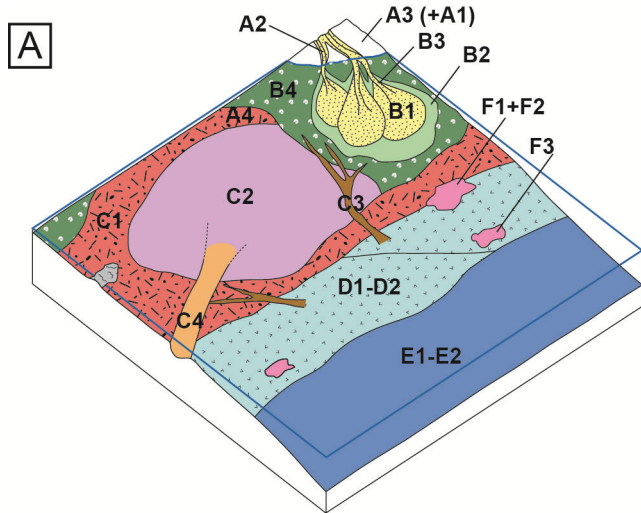


Figure 6

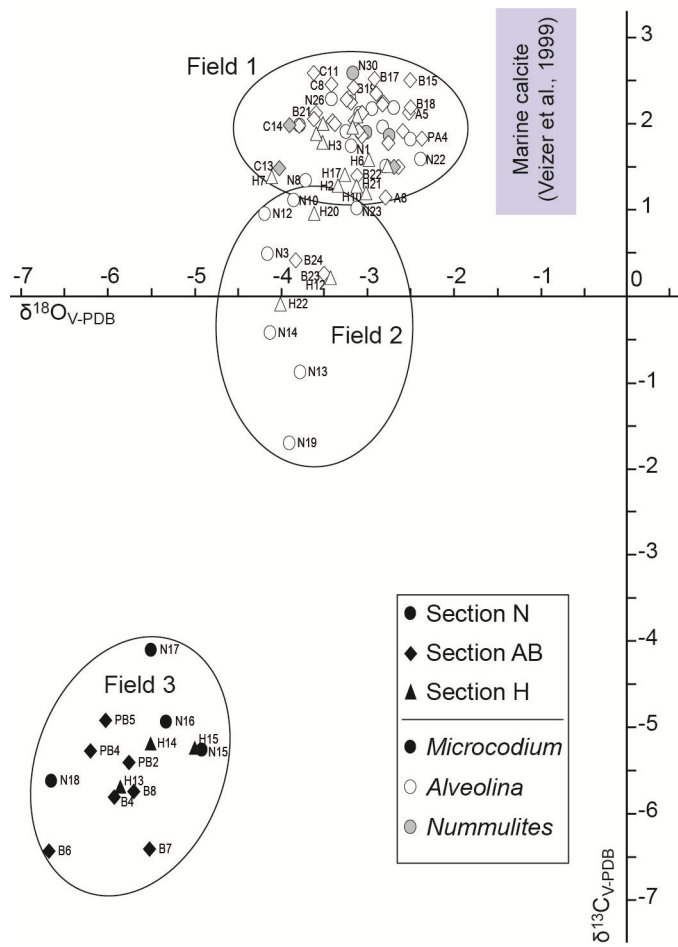


Figure 7

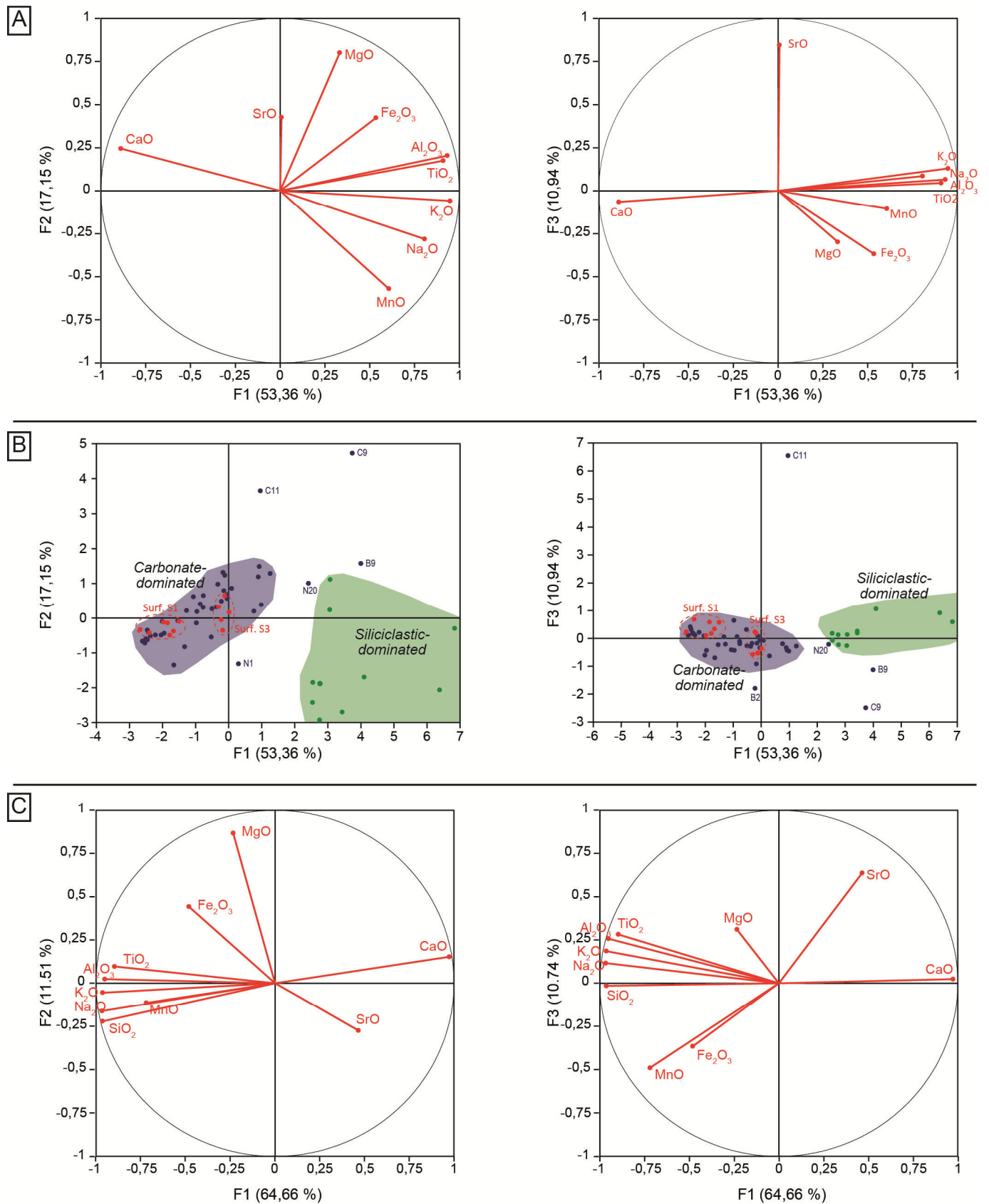


Figure 9

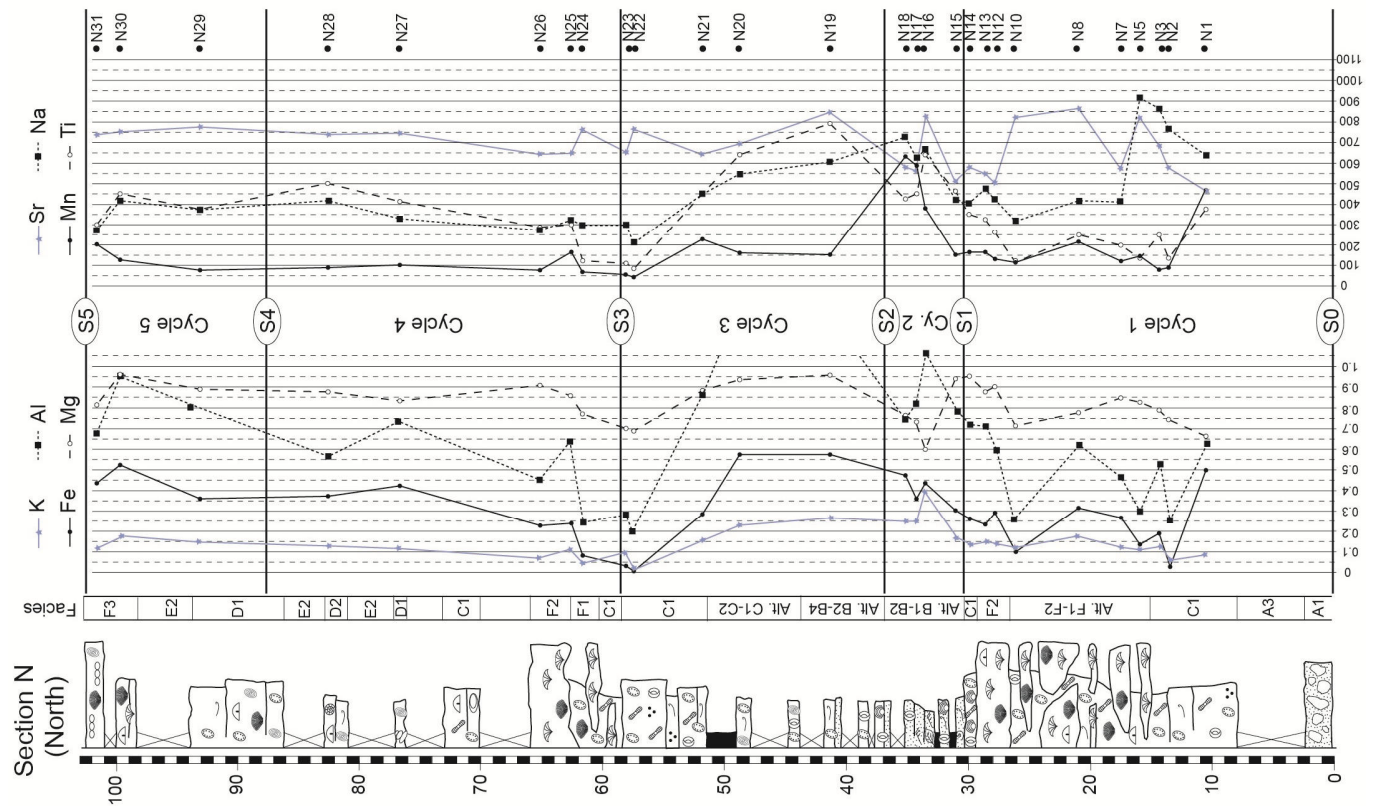
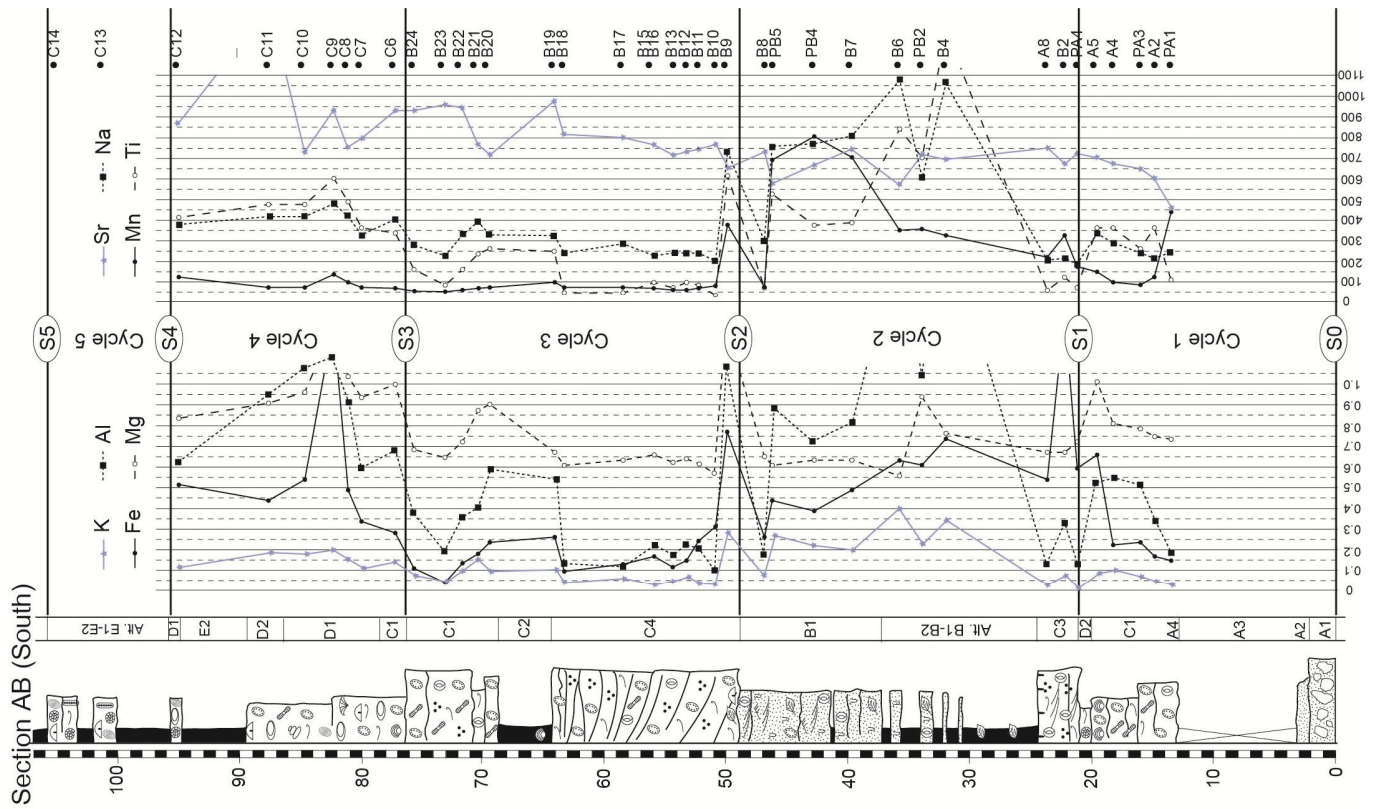


Figure 10

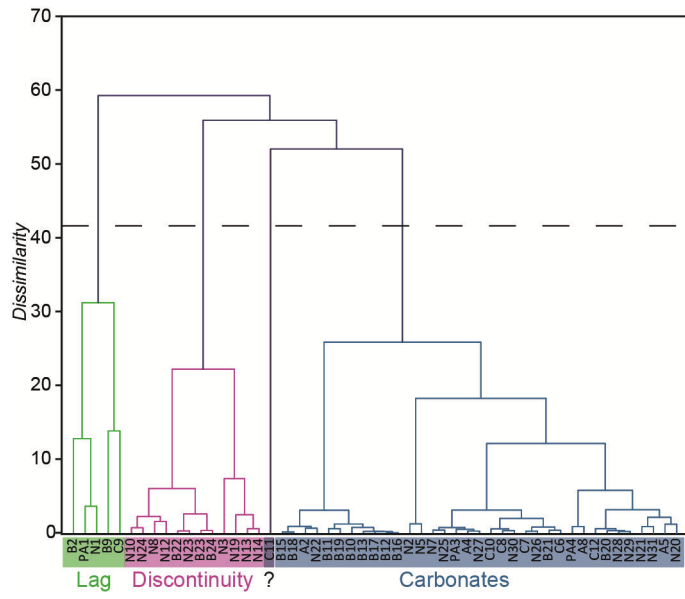


Figure 11

Sample name	Section name	Cycle	Height m	$\delta^{13}\text{C}$ ‰ v-PDB	$\delta^{18}\text{O}$ ‰ v-PDB	Fe_2O_3 %	Al_2O_3 %	CaO %	MgO %	SiO_2 %	K_2O %	MnO ppm	Na_2O ppm	SrO ppm	TiO_2 ppm	Mg/Ca Molar ratio
PA1	AB	Cy. 1	13,5	2,24	-3,19	0,143	0,187	53,85	0,729	1,16	0,03	439,50	243,99	458	113,59	2,185
A2	AB	Cy. 1	14,9	1,91	-2,58	0,164	0,340	54,59	0,745	1,35	0,05	121,88	213,84	602	367,74	2,201
PA3	AB	Cy. 1	16	2,02	-3,40	0,231	0,514	54,13	0,784	1,73	0,07	87,32	245,20	648	264,50	2,335
A4	AB	Cy. 1	18	1,85	-3,06	0,223	0,548	53,91	0,810	1,95	0,10	95,71	289,61	673	367,74	2,420
A5	AB	Cy. 1	19,7	2,12	-2,51	0,652	0,524	53,30	1,005	1,89	0,09	145,66	332,31	703	367,74	3,018
PA4	AB	Cy. 2	21,2	1,83	-2,37	0,593	0,130	53,11	0,716	1,56	0,01	176,96	187,28	725	71,15	2,176
B2	AB	Cy. 2	22,1	2,04	-3,14	1,738	0,327	52,06	0,673	1,97	0,07	322,99	215,42	676	120,10	2,088
A8	AB	Cy. 2	23,8	1,15	-2,79	0,542	0,130	53,39	0,673	1,69	0,03	220,60	208,36	747	57,20	2,037
B4	AB	Cy. 2	31,9	-5,78	-5,92	0,735	1,788	40,52	0,761	21,80	0,34	323,09	1052,9	694	1395,2	3,005
PB2	AB	Cy. 2	33,9	-5,39	-5,75	0,606	1,044	46,12	0,939	13,29	0,23	354,22	602,85	716	704,93	3,250
B6	AB	Cy. 2	35,8	-6,41	-6,68	0,631	1,691	34,32	0,554	32,90	0,40	347,67	1076,3	573	829,13	2,595
B7	AB	Cy. 2	39,8	-6,38	-5,51	0,492	0,814	46,72	0,629	13,20	0,20	704,26	799,82	743	382,85	2,173
PB4	AB	Cy. 2	42,8	-5,25	-6,20	0,386	0,724	44,48	0,637	16,51	0,22	799,48	767,99	665	370,01	2,309
PB5	AB	Cy. 2	46	-4,90	-6,02	0,438	0,882	42,59	0,607	21,34	0,27	689,93	753,25	578	528,84	2,298
B8	AB	Cy. 2	46,8	-5,72	-5,70	0,252	0,183	54,73	0,651	0,69	0,08	78,01	295,28	732	70,75	1,924
B9	AB	Cy. 3	50	1,97	-3,78	0,765	1,087	45,37	1,325	12,99	0,28	375,61	731,15	653	613,87	4,599
B10	AB	Cy. 3	50,9	1,78	-2,75	0,309	0,101	54,57	0,569	0,36	0,03	78,31	194,78	764	36,05	1,691
B11	AB	Cy. 3	52,2	2,00	-3,37	0,239	0,208	54,69	0,611	0,74	0,04	64,95	235,30	741	81,13	1,810
B12	AB	Cy. 3	53,2	2,24	-2,81	0,143	0,225	54,85	0,640	0,89	0,07	59,83	238,04	733	99,01	1,888
B13	AB	Cy. 3	54,2	2,12	-3,05	0,113	0,175	54,65	0,624	0,66	0,05	59,95	234,06	715	67,42	1,851
B15	AB	Cy. 3	56,1	2,50	-2,50	0,160	0,221	55,11	0,643	0,84	0,03	65,50	227,81	762	102,83	1,888
B16	AB	Cy. 3	56,1	2,22	-2,82	0,158	0,243	55,30	0,652	0,86	0,02	65,14	222,32	775	92,73	1,909
B17	AB	Cy. 3	58,6	2,51	-2,91	0,127	0,116	56,07	0,628	0,47	0,06	70,51	282,65	801	53,01	1,816
B18	AB	Cy. 3	63,4	2,19	-2,49	0,093	0,135	54,45	0,605	0,51	0,04	73,56	241,34	821	56,99	1,802
B19	AB	Cy. 3	64	2,42	-3,15	0,254	0,542	53,37	0,666	1,86	0,10	97,15	322,30	980	247,56	2,019
B20	AB	Cy. 3	69,8	1,50	-2,64	0,231	0,589	53,23	0,900	2,20	0,09	69,04	328,48	715	260,93	2,714
B21	AB	Cy. 3	70,7	2,12	-3,59	0,177	0,407	55,14	0,869	1,20	0,15	68,90	391,69	766	238,86	2,535
B22	AB	Cy. 3	72	1,40	-3,11	0,136	0,356	53,71	0,718	1,04	0,10	55,60	320,89	943	161,25	2,159
B23	AB	Cy. 3	73,1	0,26	-3,49	0,042	0,195	54,01	0,645	0,60	0,05	51,28	230,92	960	88,20	1,933
B24	AB	Cy. 3	75,6	0,42	-3,82	0,107	0,381	54,99	0,683	1,21	0,07	54,41	277,34	933	158,10	2,007
C6	AB	Cy. 4	77,2	2,05	-3,61	0,281	0,682	53,87	0,992	nd	0,14	65,01	398,92	932	338,12	2,949
C7	AB	Cy. 4	80,1	2,28	-3,24	0,336	0,600	52,70	0,937	nd	0,11	73,33	331,85	798	363,50	2,850
C8	AB	Cy. 4	81,2	2,45	-3,41	0,485	0,914	51,80	1,036	nd	0,15	94,95	419,66	753	489,70	3,195
C9	AB	Cy. 4	82,5	2,35	-2,89	2,120	1,133	47,55	1,462	nd	0,20	131,20	479,41	932	608,23	4,830
C10	AB	Cy. 4	84,9	1,91	-3,10	0,531	1,079	50,69	0,962	nd	0,18	75,70	411,77	734	474,97	3,035
C11	AB	Cy. 4	87,8	2,58	-3,61	0,437	0,955	51,59	0,904	nd	0,19	65,77	414,22	4567	476,16	2,810
C12	AB	Cy. 4	95,2	1,50	-2,69	0,508	0,624	53,32	0,836	nd	0,12	123,25	383,03	868	408,23	2,521
C13	AB	Cy. 5	101,3	1,49	-4,01	nd	nd	nd	nd	nd	nd	nd	nd	nd	nd	nd
C14	AB	Cy. 5	105,2	1,98	-3,90	nd	nd	nd	nd	nd	nd	nd	nd	nd	nd	nd
N1	N	Cy. 1	10,6	1,75	-3,19	0,498	0,629	56,00	0,662	nd	0,09	463,51	56,00	462	371,86	1,913
N2	N	Cy. 1	13,5	2,19	-2,69	0,028	0,257	56,00	0,745	nd	0,06	86,30	56,00	577	135,37	2,147

N3	N	Cy. 1	14,2	0,50	-4,15	0,197	0,527	56,00	0,788	nd	0,12	78,72	56,00	679	244,97	2,270
N5	N	Cy. 1	15,9	1,51	-2,79	0,136	0,299	56,00	0,829	nd	0,11	142,78	56,00	818	130,97	2,384
N7	N	Cy. 1	17,3	1,91	-3,25	0,271	0,466	56,00	0,849	nd	0,12	119,63	56,00	572	192,09	2,440
N8	N	Cy. 1	21,1	1,35	-3,71	0,313	0,620	55,30	0,777	nd	0,17	217,35	55,30	864	254,33	2,267
N10	N	Cy. 1	26	1,12	-3,85	0,103	0,259	55,09	0,717	nd	0,12	112,68	55,09	815	118,49	2,103
N12	N	Cy. 1	27,7	0,96	-4,19	0,290	0,595	53,73	0,902	nd	0,14	129,02	53,73	500	261,59	2,697
N13	N	Cy. 1	28,5	-0,87	-3,78	0,235	0,708	54,12	0,881	nd	0,15	164,12	54,12	546	316,28	2,616
N14	N	Cy. 1	29,8	-0,41	-4,12	0,262	0,719	55,20	0,953	nd	0,13	162,64	55,20	574	342,22	2,769
N15	N	Cy. 2	30,9	-5,24	-4,91	0,299	0,781	48,00	0,943	nd	0,16	149,78	48,00	513	467,96	3,141
N16	N	Cy. 2	33,5	-4,91	-5,33	0,440	1,063	39,45	0,603	nd	0,39	376,82	39,45	825	643,04	2,459
N17	N	Cy. 2	34,2	-4,08	-5,50	0,355	0,816	45,03	0,735	nd	0,25	587,53	45,03	559	445,22	2,622
N18	N	Cy. 2	35,1	-5,59	-6,65	0,468	0,748	45,43	0,762	nd	0,25	636,61	45,43	574	420,60	2,694
N19	N	Cy. 3	41,5	-1,69	-3,90	0,577	1,245	48,50	0,957	nd	0,26	150,72	48,50	839	789,19	3,154
N20	N	Cy. 3	48,8	1,96	-2,82	0,576	1,280	50,19	0,939	nd	0,23	157,80	50,19	690	643,32	2,993
N21	N	Cy. 3	51,9	2,18	-2,94	0,283	0,863	51,83	0,883	nd	0,16	223,04	51,83	642	446,14	2,734
N22	N	Cy. 3	57,1	1,59	-2,38	-0,001	0,201	55,08	0,692	nd	0,02	44,34	55,08	756	78,45	2,032
N23	N	Cy. 3	57,3	1,02	-3,12	0,038	0,284	53,29	0,705	nd	0,09	52,86	53,29	653	112,61	2,137
N24	N	Cy. 4	61,6	1,99	-3,78	0,079	0,245	53,86	0,772	nd	0,05	67,66	53,86	759	121,75	2,311
N25	N	Cy. 4	63,5	2,30	-3,20	0,240	0,638	53,48	0,858	nd	0,11	163,50	53,48	650	296,25	2,580
N26	N	Cy. 4	65	2,29	-3,41	0,227	0,453	52,95	0,906	nd	0,07	75,31	52,95	641	288,90	2,747
N27	N	Cy. 4	76,6	2,12	-3,09	0,425	0,731	52,58	0,832	nd	0,12	96,85	52,58	634	416,22	2,545
N28	N	Cy. 4	82,5	1,87	-2,75	0,366	0,566	55,11	0,878	nd	0,13	82,08	55,11	739	499,70	2,561
N29	N	Cy. 5	92,9	1,82	-2,50	0,360	0,803	53,30	0,891	nd	0,15	77,94	53,30	773	371,63	2,686
N30	N	Cy. 5	99,8	2,59	-3,17	0,528	0,951	53,05	0,958	nd	0,18	124,94	53,05	753	449,61	2,895
N31	N	Cy. 5	101,8	1,90	-3,01	0,439	0,677	54,02	0,812	nd	0,12	204,72	54,02	735	296,12	2,419
H2	H	Cy. 1	10	1,28	-3,34	nd	nd	nd	nd	nd	nd	nd	nd	nd	nd	nd
H3	H	Cy. 1	11	1,79	-3,51	nd	nd	nd	nd	nd	nd	nd	nd	nd	nd	nd
H5	H	Cy. 1	15,1	2,09	-3,11	nd	nd	nd	nd	nd	nd	nd	nd	nd	nd	nd
H6	H	Cy. 1	18,3	1,58	-2,98	nd	nd	nd	nd	nd	nd	nd	nd	nd	nd	nd
H7	H	Cy. 1	19,2	1,38	-4,10	nd	nd	nd	nd	nd	nd	nd	nd	nd	nd	nd
H8	H	Cy. 1	20,7	1,96	-3,17	nd	nd	nd	nd	nd	nd	nd	nd	nd	nd	nd
H9	H	Cy. 2	22,2	1,51	-2,76	nd	nd	nd	nd	nd	nd	nd	nd	nd	nd	nd
H10	H	Cy. 2	23,8	1,20	-3,01	nd	nd	nd	nd	nd	nd	nd	nd	nd	nd	nd
H12	H	Cy. 2	27,5	0,22	-3,42	nd	nd	nd	nd	nd	nd	nd	nd	nd	nd	nd
H13	H	Cy. 2	36,1	-5,67	-5,85	nd	nd	nd	nd	nd	nd	nd	nd	nd	nd	nd
H14	H	Cy. 2	38,4	-5,16	-5,50	nd	nd	nd	nd	nd	nd	nd	nd	nd	nd	nd
H15	H	Cy. 2	42,5	-5,21	-4,99	nd	nd	nd	nd	nd	nd	nd	nd	nd	nd	nd
H17	H	Cy. 2	44,3	1,41	-3,25	nd	nd	nd	nd	nd	nd	nd	nd	nd	nd	nd
H18	H	Cy. 3	46,7	1,88	-3,59	nd	nd	nd	nd	nd	nd	nd	nd	nd	nd	nd
H19	H	Cy. 3	48,9	2,00	-3,51	nd	nd	nd	nd	nd	nd	nd	nd	nd	nd	nd
H20	H	Cy. 3	53,4	0,97	-3,61	nd	nd	nd	nd	nd	nd	nd	nd	nd	nd	nd
H21	H	Cy. 3	54,8	1,28	-3,12	nd	nd	nd	nd	nd	nd	nd	nd	nd	nd	nd
H22	H	Cy. 3	57,9	-0,09	-4,00	nd	nd	nd	nd	nd	nd	nd	nd	nd	nd	nd

TABLE 1

Table 2A

<i>Variables</i>	<i>MgO</i>	<i>SrO</i>	<i>Fe₂O₃</i>	<i>MnO</i>	<i>Al₂O₃</i>	<i>TiO₂</i>	<i>Na₂O</i>	<i>CaO</i>	<i>K₂O</i>
<i>MgO</i>	1	0,084	0,470	-0,161	0,436	0,397	0,092	-0,038	0,247
<i>SrO</i>	0,084	1	0,036	-0,178	0,085	0,045	-0,067	0,029	0,052
<i>Fe₂O₃</i>	0,470	0,036	1	0,267	0,466	0,436	0,206	-0,412	0,369
<i>MnO</i>	-0,161	-0,178	0,267	1	0,364	0,355	0,580	-0,652	0,538
<i>Al₂O₃</i>	0,436	0,085	0,466	0,364	1	0,947	0,680	-0,759	0,894
<i>TiO₂</i>	0,397	0,045	0,436	0,355	0,947	1	0,663	-0,744	0,843
<i>Na₂O</i>	0,092	-0,067	0,206	0,580	0,680	0,663	1	-0,673	0,777
<i>CaO</i>	-0,038	0,029	-0,412	-0,652	-0,759	-0,744	-0,673	1	-0,869
<i>K₂O</i>	0,247	0,052	0,369	0,538	0,894	0,843	0,777	-0,869	1

Table 2B

<i>Variables</i>	<i>MgO</i>	<i>SrO</i>	<i>Fe₂O₃</i>	<i>MnO</i>	<i>Al₂O₃</i>	<i>TiO₂</i>	<i>Na₂O</i>	<i>CaO</i>	<i>K₂O</i>	<i>SiO₂</i>
<i>MgO</i>	1	-0,169	0,239	0,022	0,291	0,331	0,146	-0,085	0,249	0,033
<i>SrO</i>	-0,169	1	-0,303	-0,498	-0,316	-0,332	-0,319	0,408	-0,312	-0,412
<i>Fe₂O₃</i>	0,239	-0,303	1	0,408	0,386	0,359	0,327	-0,441	0,367	0,364
<i>MnO</i>	0,022	-0,498	0,408	1	0,508	0,443	0,694	-0,706	0,610	0,698
<i>Al₂O₃</i>	0,291	-0,316	0,386	0,508	1	0,957	0,931	-0,912	0,951	0,903
<i>TiO₂</i>	0,331	-0,332	0,359	0,443	0,957	1	0,862	-0,826	0,875	0,816
<i>Na₂O</i>	0,146	-0,319	0,327	0,694	0,931	0,862	1	-0,952	0,970	0,958
<i>CaO</i>	-0,085	0,408	-0,441	-0,706	-0,912	-0,826	-0,952	1	-0,941	-0,991
<i>K₂O</i>	0,249	-0,312	0,367	0,610	0,951	0,875	0,970	-0,941	1	0,943
<i>SiO₂</i>	0,033	-0,412	0,364	0,698	0,903	0,816	0,958	-0,991	0,943	1

5 Table 2